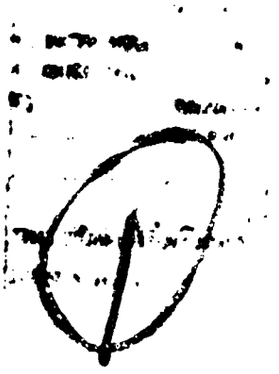

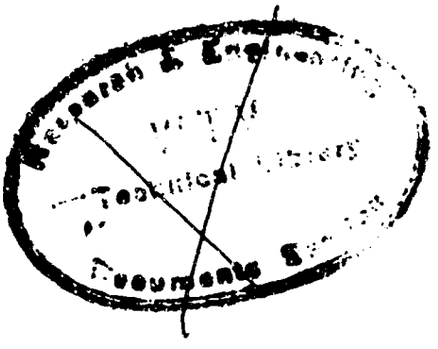

MATERIALS RESEARCH AND DEVELOPMENT

MANLABS, INC.
21 ERIE STREET
CAMBRIDGE 39
MASSACHUSETTS

74

SLOW CRACK GROWTH IN GUN TUBES

by

R. D. Large, S. A. Kulin and
B. S. Lement

Final Report

Contract No. DA-30-144-AMC-1639(W)

Submitted to:

Watervliet Arsenal

Attention: SWEWV-RDI
Mr. W. Colangelo
Project Monitor

August 1967

MATERIALS RESEARCH AND DEVELOPMENT

21 ERIE STREET
CAMBRIDGE 39
MASSACHUSETTS

TABLE OF CONTENTS

TABLE OF CONTENTS (CONT)

LIST OF ILLUSTRATIONS

LIST OF ILLUSTRATIONS (CONT)

LIST OF TABLES

ABSTRACT

Crack growth rates, in various environment during high stress-low cycle fatigue testing, load testing and continuous loading were measured in three production gun steels, Marage 250 and Republic 9-4-30. These results were combined with measured mechanical properties and fracture toughness parameters for comparison with service behavior.

I. INTRODUCTION

A. Background

The failures of large gun tubes in service are believed to involve the following stages of cracking: a) formation of a "crazing" pattern on the bore surface after a relatively few rounds of firing, b) preferential slow crack growth in a radial direction on continued firing and c) unstable crack growth resulting in complete fracture through the gun tube wall during the final round of firing. The initial stage of crack formation is apparently due to the combined effects of varying internal pressure, hot gases and thermal cycling of the bore surface during each round of firing. With current gun tubes, it does not seem possible to prevent this stage of crack formation. The second stage, which involves slow crack growth, has not been sufficiently investigated, but may be due to corrosion fatigue effects associated with the alternation of internal pressure and the formation of hot gases during firing. This intermediate stage usually involves preferential growth of cracks that initiate along land fillets where the maximum service stress is developed. These cracks progress in a radial direction from the bore to the outside surface until a critical crack length is reached that depends on the peak internal pressure, fracture toughness and design of the gun tube. The final stage involves unstable crack growth, which results in either longitudinal rupture of the gun tube wall or "blowing up" of the gun tube into many fragments.

Since a gun tube is usually serviceable until the final stage of cracking occurs, the service life may be considered to depend on the number of firings required for a radial crack to reach a critical size. For a given gun tube design and peak internal pressure developed during firing, the service life should therefore

depend on both the rate of slow crack growth and the magnitude of the critical crack size. For gun tubes of the same fracture toughness level and consequently the same critical crack size, the tube with the lowest rate of slow crack growth would be expected to give the longest service life. This follows since more firing rounds would be required to reach the critical crack size than for a tube with a faster rate of growth. However, for gun tubes of varying fracture toughness levels, either the rate of slow crack growth or the critical crack size may determine which tube gives the longest service life.

B. Program Scope

Although the phenomenon of slow crack growth in gun tubes is not understood, it is probably related to both the fracture toughness and fatigue characteristics under corrosive conditions. The present program constituted an investigation of slow crack growth in currently used as well as potential gun steel compositions. The main objective of this program was to determine the slow crack growth characteristics of selected gun steels at stress levels below that corresponding to pop-in under plane strain conditions. Determinations were made of slow crack growth in precracked bend specimens under continuous, constant and cyclic loading, using both optical and electrical potential measurements to follow crack extension. In order to show possible stress corrosion and corrosion fatigue effects, the tests were conducted using dry argon and distilled water as environmental extremes.

C. Materials

The materials selected for this program consist of a 3% nickel steel* finished 175mm gun tube (no. 1131) that was subjected to service firings at an

*Similar in composition to 4337 mod. except for lower carbon content (0.32% vs. 0.37%), higher nickel content (3% vs. 1.8%) and higher chromium content (1.27% vs. 0.85%).

estimated peak internal pressure of 50 ksi followed by pressure cycling at Watervliet Arsenal from zero to 50 ksi until failure occurred, a 4337 mod. steel finished 175mm tube (no. 733) that was subjected to approximately the same number of firings and the same peak internal pressure as no. 1131, but failed in service, a 3% nickel steel* unfinished 175mm gun tube (no. 1007) in the heat treated condition, a Marage 250 steel billet in the soft condition, a Republic 9-4-20 (Cr, Mo) steel plate in the hot rolled condition and a Republic 9-4-30 steel plate in the hot rolled condition. General information on these materials is given in Table 1. The three gun tubes were tested in the as-received condition (already heat treated), whereas the Marage 250, the Republic 9-4-20 (Cr, Mo) and the Republic 9-4-30 steels were heat treated at ManLabs prior to mechanical testing.

*Similar in composition to 4337 mod. except for lower carbon content (0.32% vs. 0.37%), higher nickel content (3% vs. 1.8%) and higher chromium content (1.27% vs. 0.85%).

TABLE I

GENERAL INFORMATION ON PROGRAM MATERIALS

Steel	Type	Description	Source	As-Received Condition	Service History
1131	3% nickel	175mm gun tube made from forging	Armco Steel Corp., National Supply Div.	finished, used in service	fired 363 rounds in service and subjected to 9685 cycles at approx. 50 ksi pressure at Watervliet Arsenal until failure occurred.
733	4337 mod.	175mm gun tube made from forging	Bethlehem Steel Company	finished, used in service	fired 373 rounds, failure occurred in service.
1007	3% nickel	175mm gun tube made from forging	Bethlehem Steel Company	heat treated, rough machined	not fired, unfinished gun tube.
09132	Marage 250	6-1/8 inch square forged billet	Vanadium Alloys Steel Company	soft	none
	9-4-20 (Cr, Mo)	6 inch wide by 2 inch thick rolled plate	Republic Steel Company	annealed	none
	9-4-30	6 inch wide by 2 inch thick rolled plate	Republic Steel Company	annealed	none

II. CHARACTERIZATION OF MATERIALS

A. Chemical Composition

According to the suppliers' specifications, the composition limits of the conventional gun tubes investigated are as follows:

Steel	C	Mn	P max	S max	Si	Ni	Cr	Mo	V
3% nickel	.28/38	.30/.70	.015	.015	.15/.50	2.50/3.75	.50/1.20	.40/1.00	.06/.15
4337-mod.	max .45	.40/.90	.025	.025	.10/.30	1.00/2.50	.50/2.00	.35/.85	max .25

As shown in Table 2, both the suppliers' and check chemical analyses carried out by ManLabs on tubes no. 1131, 733 and 1007 indicate that their chemical compositions fall within the specification limits. The check analyses made on these tubes essentially confirm those reported by the respective suppliers. It is of interest to note the large difference in nickel content between tubes no. 1131 and 1007 and tube no. 733. With respect to the no. 09132 Marage 250 billet, relatively large differences were found in nickel content (17.87% vs. 18.45%) and in cobalt content (8.51% vs. 7.70%) by the two analyses. This indicates possible segregation effects although different and possibly inaccurate techniques of chemical analysis may have been used.

Although the Republic 9-4-20 (Cr, Mo) has a carbon content corresponding to HP-9-4-25, the amount of alloying elements in the two steels are quite different.

B. Nonmetallic Inclusion Content

Nonmetallic inclusion ratings of the program steels based on ASTM E45-63, Method A are given in Table 3. The maximum severity (worst field) and average severity, which are listed for each type of inclusion, are based on examination of 64 fields at 100X in a longitudinal specimen, located adjacent to the bore surface for the gun tubes.

TABLE 2

CHEMICAL COMPOSITION OF PROGRAM STEELS

Steel	C	Mn	P	S	Si	Ni	Cr	Mo	V	Co	Others	Analyzed By
1007	0.35	0.46	0.003	0.007	0.27	3.000	0.80	0.76	0.124			ManLabs*
	0.37	0.50	0.010	0.007	0.45	3.15	0.87	0.64	0.11			Bethlehem
1131	0.35	0.47	0.007	0.006	0.25	3.05	0.80	0.68	0.124			ManLabs*
	0.35	0.44	0.010	0.007	0.39	3.12	0.80	0.65	0.08			National Supply
733	0.36	0.70	0.010	0.008	0.18	1.83	1.12	0.84	0.19			ManLabs*
	0.35	0.70	0.013	0.009	0.19	1.81	1.16	0.68	0.12			Bethlehem
Marage 250	0.02	0.08	0.003	0.008	0.06	18.45		4.74		7.70	0.32 Ti 0.04 Al 0.012 Zr 0.003 B	Vanadium Alloy
	0.015	0.02	0.005	0.006	0.05	17.87		4.71		8.51	0.41 Ti	ManLabs*
9-4-20	0.25	0.26	0.003	0.010	0.05	6.91	1.03	0.97	0.09	4.11	0.10 Al	ManLabs*
	0.25	0.32	0.004	0.007	0.01	7.19	1.01	1.03	0.09	3.90	0.01 Al	Republic
(Cr, Mo)												
9-4-30	0.33	0.03	0.005	0.010	0.03	7.11	1.07	0.65	0.09	4.11		ManLabs*

*Submitted to Saunders Associates for analysis.

TABLE 3

NONMETALLIC INCLUSION RATINGS OF PROGRAM STEELS

Steel	Severity Basis	ASTM E45-65, Method A Severity Ratings							
		Type A		Type B		Type C		Type D	
		Thin	Heavy	Thin	Heavy	Thin	Heavy	Thin	Heavy
1131	maximum*	0	0	1.5	1	0	1	2	1+
	average**	0.0	0.0	0.1	0.0	0.0	0.1	0.5	0.2
733	maximum*	1	1	1	0	2	1.5	2	1++
	average**	0.1	0.0	0.0	0.0	0.1	0.0	0.4	0.1
1007	maximum*	2	1	1	0	1	1.5+++	2	1++++
	average**	0.2	0.0	0.0	0.0	0.1	0.1	0.5	0.1
Marage 250	maximum	1	4	5	1	2	1	2	1
	average	0.0	0.1	1.0	0.1	0.1	0.0	0.5	0.2
9-4-30	maximum	0	0	1	0	1	0	3	0
	average	0.0	0.0	0.0	0.0	0.4	0.0	1.9	0.0

*Severity of worst field using ASTM Plate III.
**Averages are based on examination of 64 fields in a single longitudinal specimen.
+One type D inclusion found about 0.64 mil in diameter.
++Two type D inclusions found about 0.60 mil in diameter.
+++Two type C inclusions found about 0.54 mil in thickness.
++++One type D inclusion found about 0.60 mil in diameter.

All of the program steels appear to be relatively inclusion free with the exception of the 250 grade Maraging steel.

C. Macroexamination

Transverse slices of tubes no. 1131, 733 and 1007 were macroetched in 50% HCl - 50% H_2O for 20 minutes at 165°F. Other than the service cracks in tubes no. 1131 and 733, no evidence was found of defects such as seams, cracks or flakes. However, some evidence of dendritic structure remaining from the original ingot was found in all three tubes indicating a relatively low level of hot working.

Macroexamination of the Marage 250, the Republic 9-4-30 and the Republic 9-4-20 (Cr, Mo) revealed no defects.

D. Heat Treatment of Program Steels

Table 4 lists the heat treatments given the program steels and the resulting 0.1% yield strengths. The heat treatments given tubes no. 1131, 733 and 1007 were production heat treatments, while those given the Marage 250, Republic 9-4-30 and Republic 9-4-20 (Cr, Mo) were performed at ManLabs.

The 0.1% yield strength of 164 ksi for Republic 9-4-20 (Cr, Mo) is the highest yield strength obtainable in this steel utilizing a conventional quench and temper heat treatment. Since this yield strength does not reach the desired yield strength level of 175 to 185 ksi, testing of this steel was discontinued following precracked impact testing (Section IIB).

It should be noted that a 10 hour age instead of a 3 hour age was necessary to obtain the desired yield strength level of 240-250 ksi for the Marage 250.

The tempering temperature of 1100°F for HP-9-4-30 was determined by the method described in Section I E.

TABLE 4

HEAT TREATMENT PROCEDURES FOR PROGRAM STEELS

Steel No.	Heat Treatment	0.1% Offset Yield Strength ksi
1131*	a) austenitize 1550°F, 5 hours, w. q. b) temper 1025°F, 8 hours, w. q.	181
733*	a) austenitize 1640°F, quench b) straighten 960°F c) temper 960°F	186
1007*	a) austenitize 1550°F, quench b) straighten 1040°F c) temper 1040°F	175
Marage 250	a) solution anneal 1550°F, 1 hour, a. c. b) age 900°F, 10 hours	241
9-4-20 (Cr, Mo)	a) austenitize 1625°F, 1 hour, o. q. b) temper 1000°F, 1 + 1 hours	164
9-4-30	a) austenitize 1550°F, 1 hour, ln. q. b) temper 1100°F, 1 + 1 hours	182

*Production heat treatment.

E. Heat Treatment of Republic 9-4-30

Oversized tensile blanks of Republic 9-4-30 steel were heat treated as below before final machining.

1. 1500°F 1 hour; oil quench; liquid nitrogen quench.
2. Temper 1 hour; liquid nitrogen quench.
3. Temper 1 hour; air cool

The tempering temperatures used were 950°F, 1000°F, 1050°F 1100°F and 1150°F. Two tensile specimens were tempered at each temperature.

Figure 1 shows the variation of the tensile properties with tempering temperature for the Republic 9-4-30 alloy. A tempering temperature of 1100°F gives the required 0.1% offset yield strength of 180,000 psi.

F. Tensile Tests

The specimen geometry for tensile testing of the program steels is shown in Figure 2. All tensile tests were performed on a Baldwin 60 BTE Universal Tensile Machine. Autographic stress strain curves were recorded for each specimen using a microformer averaging extensometer. At least two tensile specimens were tested for each steel in both the longitudinal and transverse direction.

Table 5 reports the results of tensile testing. The 0.1% transverse yield strengths fall in the range 175 to 186 ksi with the exception of the Marage 250 steel and the 9-4-20 (Cr, Mo). Specification MIL-T-10458C(MR), 28 October 1963 (which covers forgings) specifies a minimum reduction in area of 19% in the transverse direction and 35% in the longitudinal direction for steels having a 0.1% yield strength of 175-185 ksi. The three gun tubes and the Republic 9-4-30 all satisfy this requirement. However, both on this basis and on the basis of per cent elongation,

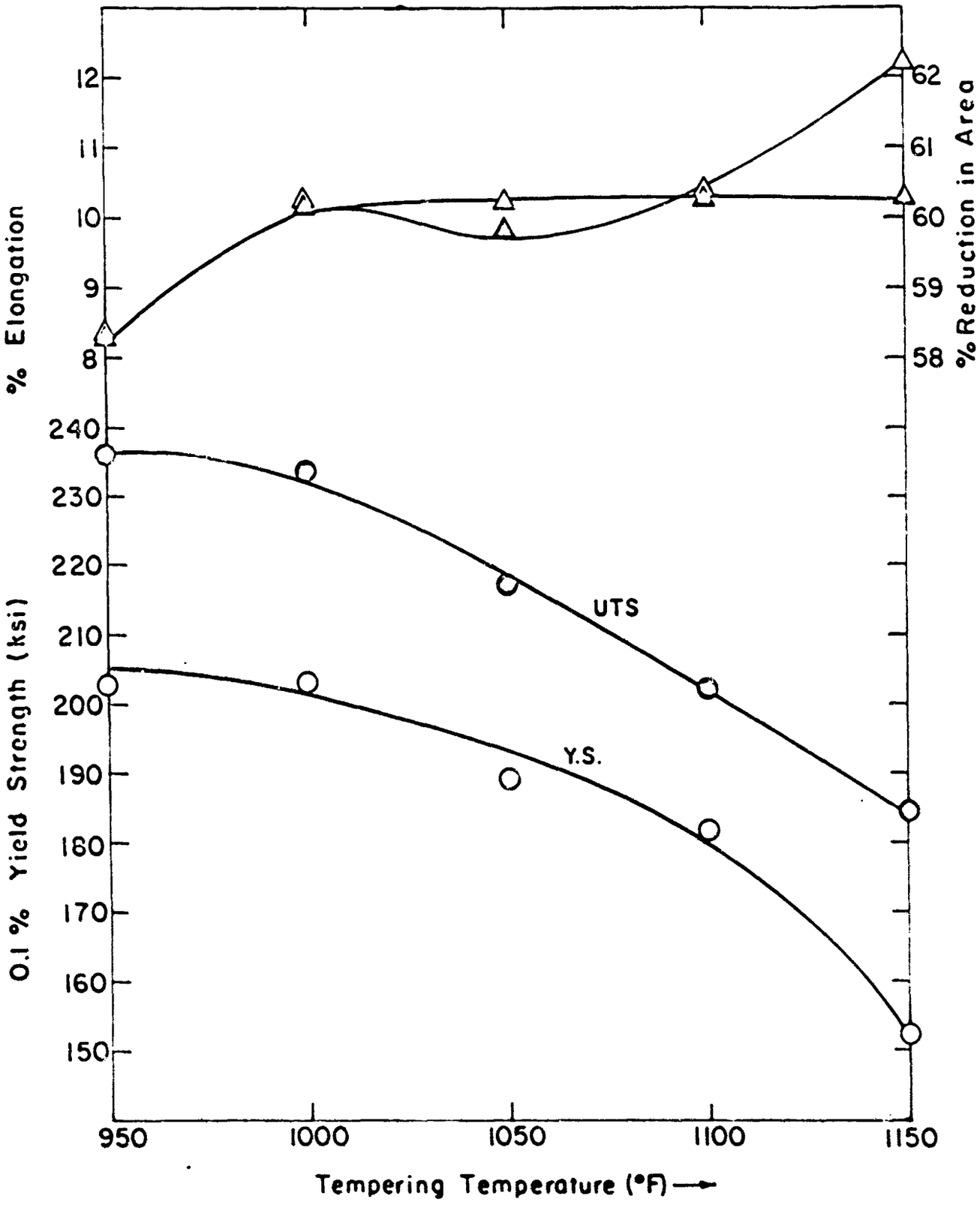

Figure 1. Tensile Properties of Republic 9-4-30 As a Function of Tempering Temperature from 950°F to 1150°F.

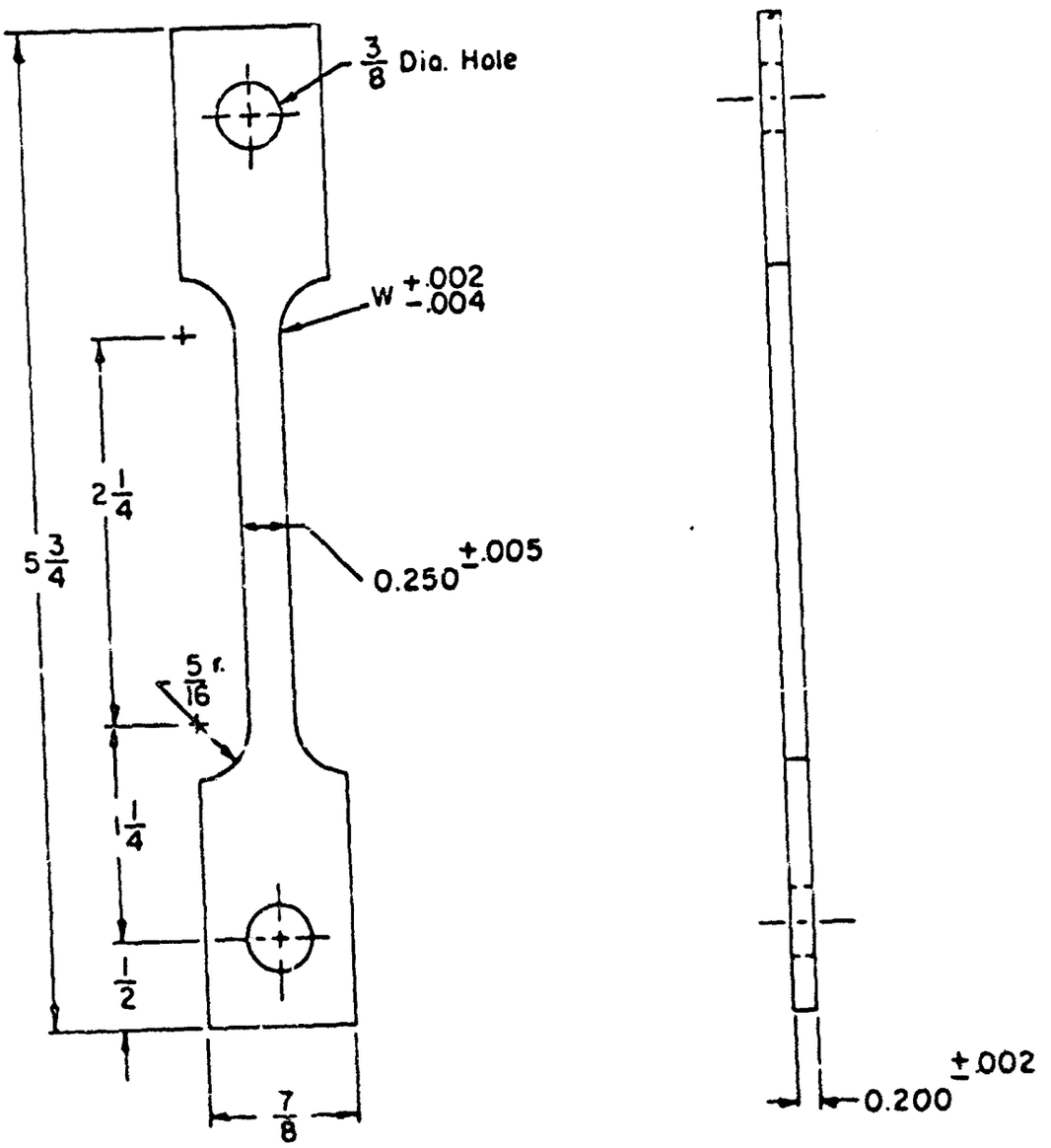

Figure 2. Tensile Specimen Geometry.

TABLE 5

TENSILE PROPERTIES OF PROGRAM MATERIALS

Steel No.	Orientation	0.1% Offset Yield Strength ksi	0.2% Offset Yield Strength ksi	Ultimate Tensile Strength ksi	True Fracture Stress ksi	Elongation %	Red in Area %	Strain Hardening Parameters n	K/ksi
1131	trans	181	186	201	307	10.5	49.7	0.044	227
	long	136 to 181	150 to 186	194 to 202	312 to 337	9.5 to 10.8	51.4 to 58.8		
733	trans	186	193	215	270	7.7	27.2	0.061	283
	long	179	184	199	338	10.0	57.0		
1007	trans	175	181	196	255	8.6	32.8	0.049	233
		173	178	195	293	9.4	48.5		
Marage 250	trans	241	253	258	307	3.7	31.0	0.080	368
	long	245	252	259	377	6.3	57.3		
9-4-20 (Cr, Mo)	trans	164	178	212	394	12.0	67.3		
	long	161	174	215	400	12.3	66.9		
9-4-30	trans	181.5	187.4	201.8	351.3	10.4	62.5	0.053	246
	long	171.9	187.2	206.7	344.1	10.7	59.6		

the Republic 9-4-30 is superior to all of the steels at the 180 ksi yield strength level. The highest ductility amongst the three gun tubes is exhibited by no. 1131 while no. 733 is lowest.

The large variation of tensile properties in tube no. 1131 in the longitudinal direction is thought to be due to residual stresses and/or segregation, although no definite conclusion may be drawn without further testing.

G. Charpy Impact Tests

Table 6 lists the standard Charpy impact energies at room temperature and -40°F in both the longitudinal and transverse direction. These data were obtained by testing the program steels, in duplicate for each condition and test temperature, in a ManLabs CIM-24 Impact Machine using the specimen geometry shown in Figure 3.

Specification no. MIL-T-10458C(MR), calls for minimum Charpy impact energies of 11 and 19 ft/lbs at -40°F in the transverse and longitudinal directions, respectively. In the former case, the crack propagates in a radial direction in a longitudinal plane whereas in the latter case, crack propagation is in a radial direction in a transverse plane.

Reference to Table 6 shows that tube no. 733 does not meet this specification and tube no. 1007 is marginal. Tube no. 1131, while acceptable, is inferior to the Republic 9-4-30. The Republic 9-4-20 (Cr, Mo) has exceptionally high impact energy at a lower yield strength, while the 250 grade Maraging steel is quite low. Note should be made of the large variation in transverse and longitudinal Charpy energies in tube no. 733 and the Marage 250.

TABLE 6

CHARPY IMPACT TESTS OF PROGRAM STEELS

Steel No.	Orientation	Test Temp	W (ft-lbs)
1131	trans	+75	25.3
		-40	14.6
	long	+75	31.0
		-40	20.2
733	trans	+75	10.5
		-40	6.4
	long	+75	29.9
		-40	20.8
1007	trans	+75	17.6
		-40	10.4
	long	+75	25.8
		-40	17.5
Marage 250	trans	+75	5.0
		-40	5.4
	long	+75	26.6
		-40	15.6
9-4-20 (Cr, Mo)	trans	+75	41.1
		-40	34.1
9-4-30	trans	+75	27.0
		-40	20.8
	long	+75	27.9
		-40	23.6

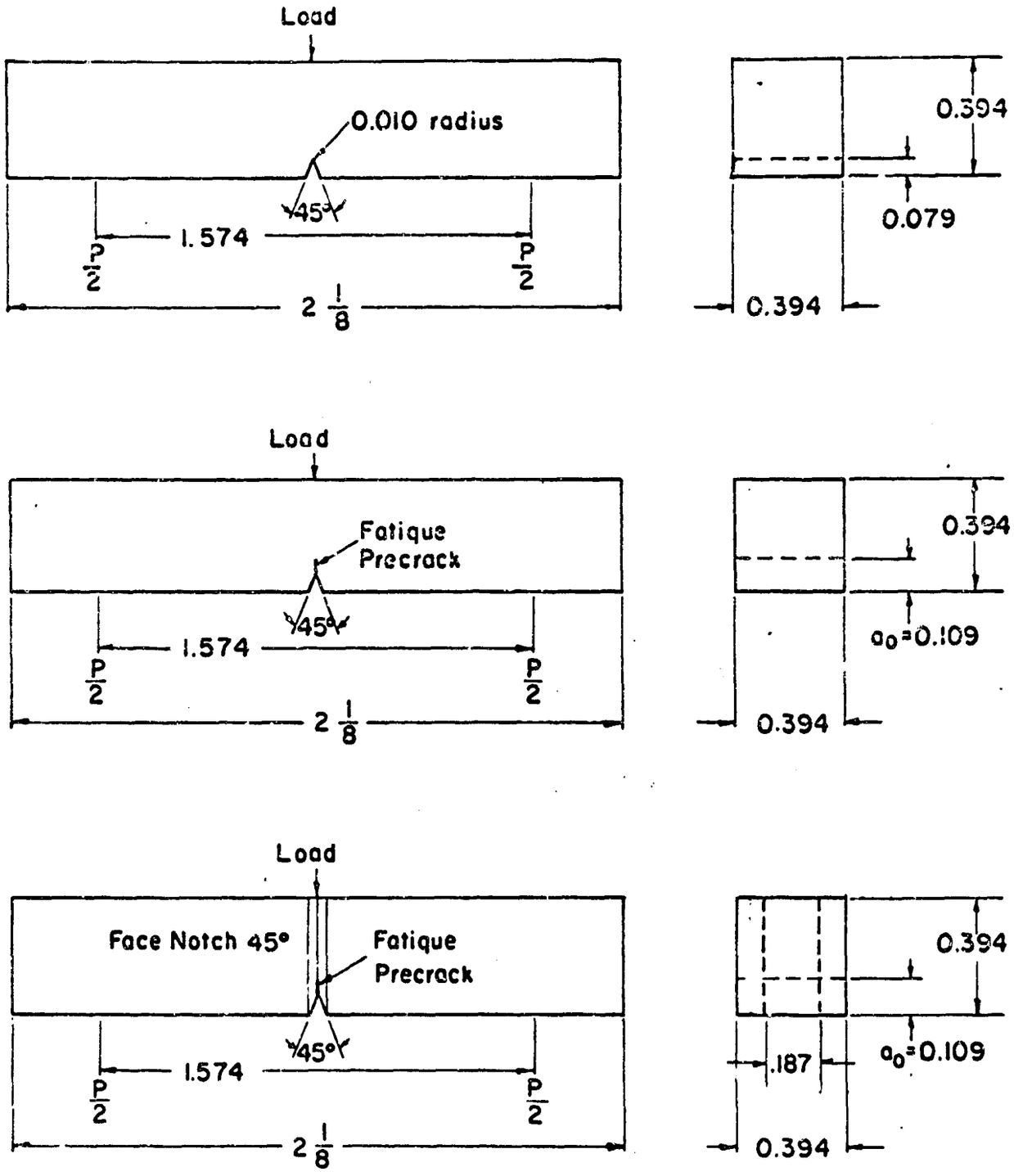

Figure 3. Conventional, Precracked and Precracked Face Notched Impact and Slow Bend Specimens.

III. PRECRACKED IMPACT AND SLOW BEND TESTS

A. Procedure

Precracked Charpy impact and slow bend tests were carried out on specimens of the design shown in Figure 3. Fatigue precracking to a depth of about 30 mils below the V-notch was carried out in a ManLabs FCM-300 machine operating at 1800 rpm. The impact and slow bend tests were carried out in ManLabs CIM-24 and SB-750 testing machines, respectively.

B. Results of Precracked Charpy Impact Tests

Precracked Charpy impact tests (PCI) were conducted in the transverse direction at test temperatures of +75°and -40°F in air. As shown in Table 7, the $(W/A)_{pci}$ values fall in the range of 411 to 2676 inch-lbs/inch^2 at +75°F and 158 to 2174 inch-lbs/inch^2 at -40°F. The order of decreasing toughness being 9-4-20 (Cr, Mo), 1131, 9-4-30, 1007, 733, Marage 250. Based on the $(W/A)_{ci}$ results of Table 2, the ratios of $(W/A)_{pci}$ to $(W/A)_{ci}$ fall in the range of 63 to 85% except for tube no.733 at -40°F (26%). Since the drop in impact toughness of tube no.733 with decrease in test temperature is more pronounced with a PCI than with a CI test, it appears that lowering the test temperature has a great effect on crack propagation in this steel.

C. Results of Precracked Slow Bend Tests

Precracked slow bend tests (PSB) were carried out in the transverse direction at +75°F in a dry argon atmosphere. The specimen was subjected to three point loading at a deflection rate of 0.0125 inch/minute. As shown in Table 3, it was found that the $(W/A)_{psb}$ values are in the range of 406 to 1844 inch-lbs/inch^2. The order of decreasing toughness being the same as for the PCI test.

TABLE 7

PRECRACKED IMPACT AND SLOW BEND TESTS OF PROGRAM MATERIALS IN THE TRANSVERSE DIRECTION

Steel No.	Test Temp.	$(W/A)_{PCI}$ in-lbs/in^2	$(W/A)_{PCI}/(W/A)_{CI}$ %	$(W/A)_{SB}$* in-lbs/in^2
1131	+75	2055	84	1060
	-40	1015	72	----
733	+75	644	63	507
	-40	158	26	---
1007	+75	1317	77	865
	-40	803	80	---
Marage 250	+75	411	85	406
	-40	355	67	---
9-4-20 (Cr, Mo)	+75	2676	67	1844
	-40	2174	66	----
9-4-30	+75	1793	69	1093
	-40	1261	63	----

*Tested in dry argon.

IV. PRECRACKED FACE NOTCHED SLOW BEND TESTS

A. Procedure

In an attempt to approach plane strain conditions, precracked face notched slow bend tests (PFNSB) were carried out on specimens of the design shown in Figure 1C. Precracking was accomplished in the same way as for the PCI and PSB test specimens and was carried out prior to face notching. Using three point loading, slow bend tests of these specimens were carried out in the transverse direction at a deflection rate of 0.0125 inch/minute in dry argon at +75°F.

B. Effect of Face Notch Depth

The effect of face notch depth on $(W/A)_{pfnsb}$ was determined for tube no. 1007. The notch depth was expressed as the ratio of the effective thickness (B_n) to the actual thickness (B). An IBM 1130 computer was used to determine the curve that would best fit the $(W/A)_{pfnsb}$ vs. B_n/B data. The least squares solution for such a curve was found to be as follows:

$$(W/A)_{pfnsb} = 451 + 868\,(B_n/B) - 2125\,(B_n/B)^2 + 2691\,(B_n/B)^3 - 1027\,(B_n/B)^4 \qquad (1)$$

A plot of Eq. (1) is shown in Figure 4. The average slope is about 245 over the range of (B_n/B) values from 0.15 to 0.6 and increases to about 525 for the range of (B_n/B) values from 0.6 to 1.0. Considered from the standpoint of increasing face notch depth $(W/A)_{pfnsb}$ decreases markedly until the effective thickness is reduced about 40%; and then decreases more gradually with increased notch depth. Although a constant value of $(W/A)_{pfnsb}$ was not attained with the tube no. 1007 material, it was decided to standardize on a (B_n/B) ratio of 0.5 for comparing the plane strain fracture toughness values of the program materials. As shown by Kalish and Kulin (1*),

*Underscored numbers in parentheses designate References given at end of report.

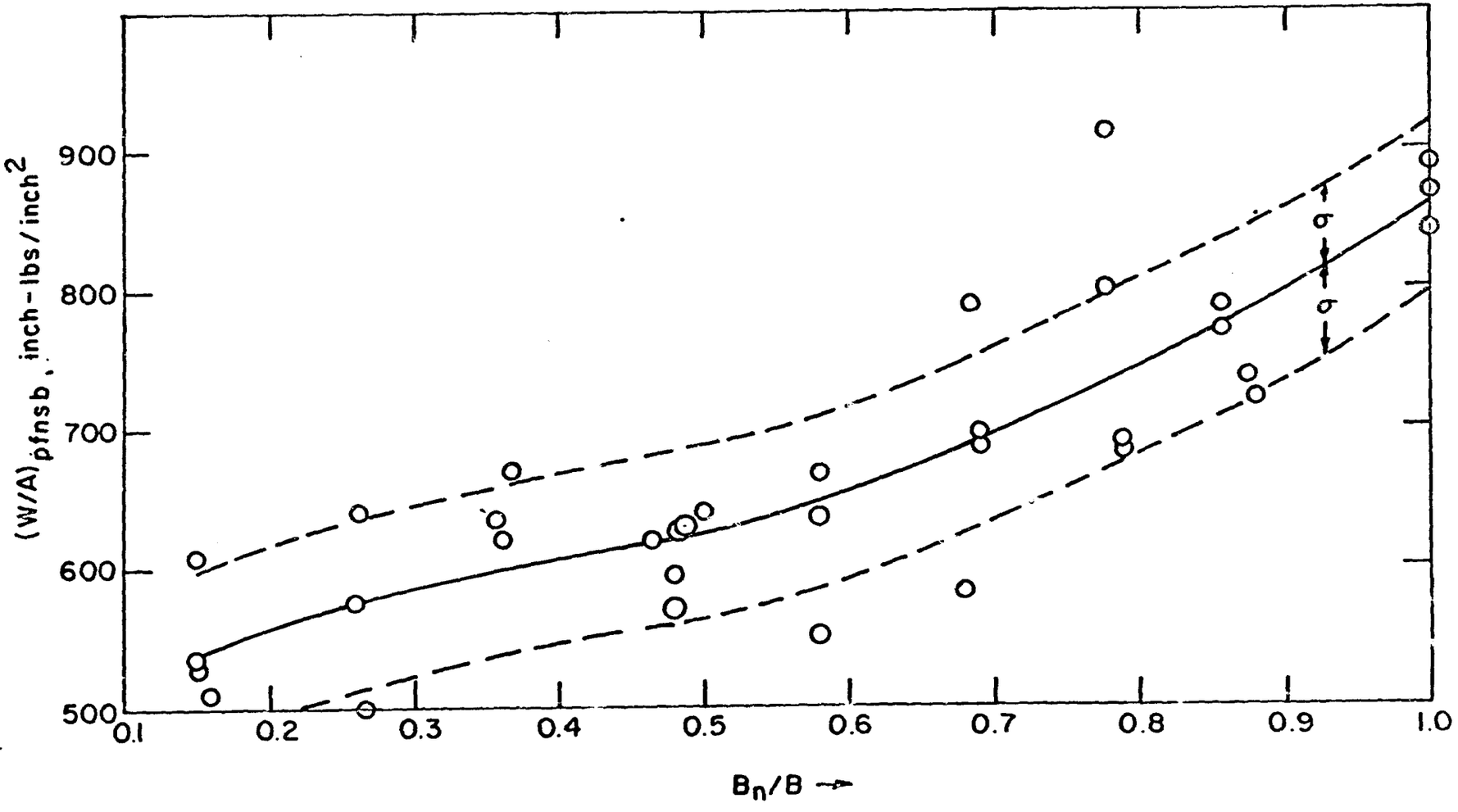

Figure 4, Variation of Plane Strain Fracture Toughness Parameter, $(W/A)_{pfnsb}$, with Ratio of Effective to Actual Thickness, B_n/G, as Determined by Least Squares Fit of Data on Tube No. 1007 Using IBM 1130 Computer.

$(W/A)_{pfnsb}$ at $B_n/B = 0.5$ correlates with other plane strain fracture toughness parameters.

For $B_n/B = 0.5$, the following $(W/A)_{pfnsb}$ values in the transverse direction were obtained:

Material	0.1% Yield Strength ksi	$(W/A)_{pfnsb}$ inch-lbs/inch^2
Tube no. 1131	181	760
Tube no. 733	186	500
Tube no. 1007	175	610
Marage 250	241	325
Republic 9-4-30	181	825
		?

These experiments showed that tube no. 1131 has a higher plane strain fracture toughness level than tube no. 733 with tube no. 1007 being intermediate in plain strain fracture toughness. More important, the order of decreasing fracture toughness, as plain strain conditions are approached, does not change among the three gun steels. Republic 9-4-30 exhibits the highest level of fracture toughness on this basis.

IV. DUCTILE-BRITTLE TRANSITION

PCI specimens of steels no. 733, 1131 and 1007 were tested in impact at eight temperatures from -80°F to 200°F and also at -320°F. Figure 5 shows the resulting values of precracked Charpy impact energy $(W/A)_{PCI}$, as a function of testing temperature for the three gun steels.

The transition temperature for each steel was defined as the test temperature at which 50% of the super transitional value of $(W/A)_{PCI}$ was attained. Comparing the three gun steels on the basis of super transitional $(W/A)_{PCI}$ and transition temperature, the results are given below in Table 8.

TABLE 8

TRANSITION DATA

Tube No.	Super Transitional $(W/A)_{PCI}$ inch-lbs/inch^2	Transition Temperature °F
1131	2040	-32
1007	1460	-43
733	1100	+41

The results indicate that both tubes no. 1131 and 1007 are superior to tube no. 733 on the basis of both super transitional $(W/A)_{PCI}$ as well as transition temperature. Although tube no. 1131 has a considerably higher super transitional $(W/A)_{PCI}$ than tube no. 1007, its transition temperature is slightly higher than tube no. 1007. In addition, it should be noted that at room temperature, both tubes no. 1007 and 1131 have achieved their super transitional level of $(W/A)_{PCI}$ while tube no. 733 has reached only 70% of this level of toughness.

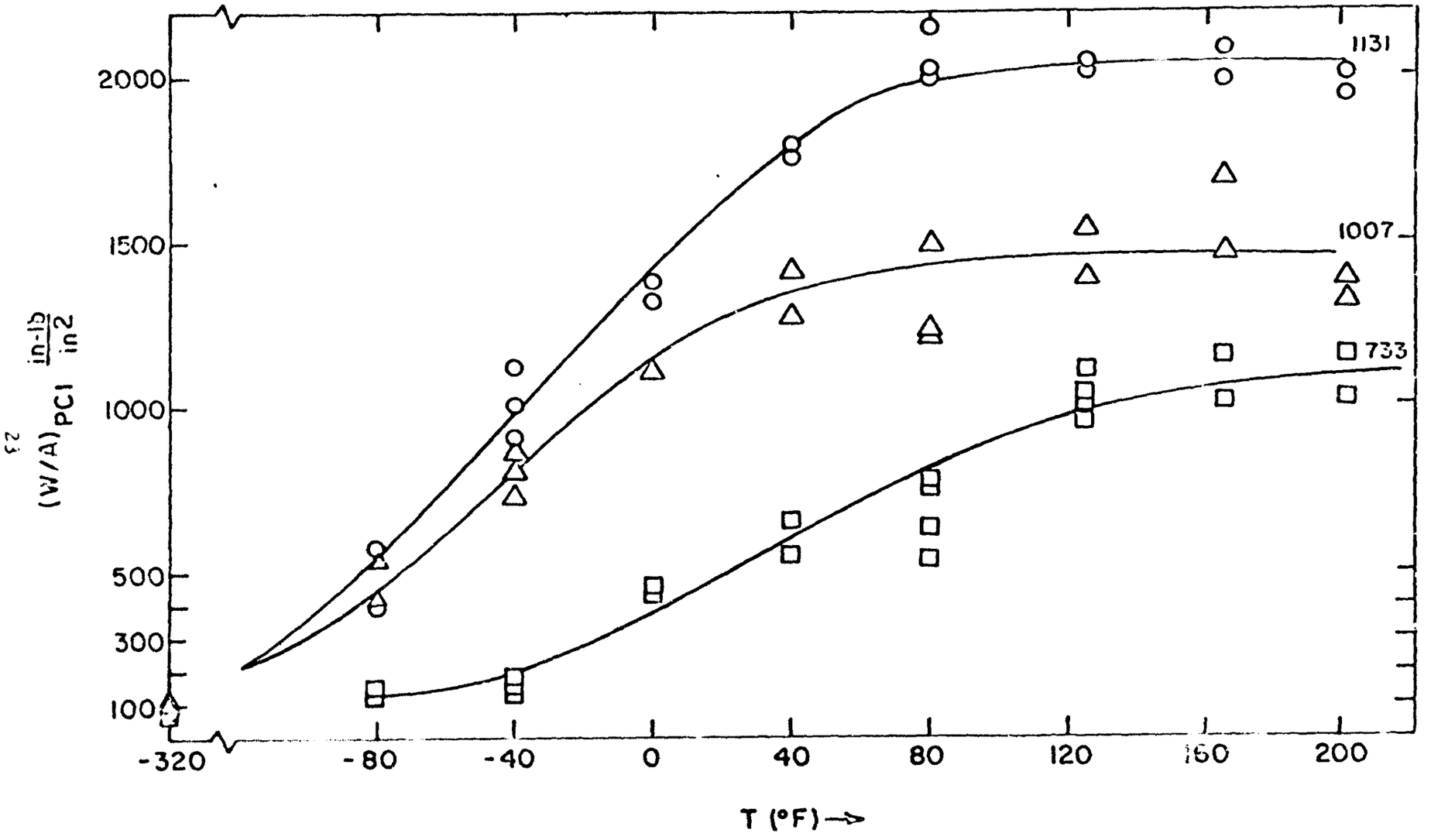

Figure 5. Ductile-Brittle Transition in Tubes No. 733, 1131 and 1007.

V. TEMPER EMBRITTLEMENT

A. Background

For the purposes of this program, it was assumed that temper embrittlement is caused by a reversible grain boundary phenomena such as grain boundary film formation, precipitation or segregation, i.e., classical temper embrittlement as opposed to the lower temperature, nonreversible embrittlement. Hence, if a gun tube in question arrived in a temper embrittled condition, reheating to a temperature at or slightly above the tempering temperature followed by a water quench should substantially alleviate the embrittlement. Conversely, if the gun tube in question arrived in a nontemper embrittled condition, slow cooling through the embrittleling range would induce some temper embrittlement if the tube is susceptible.

B. Procedure

CI specimens of steels 733, 1007 and 1131 were subjected to the following heat treatments:

1. $1050^{\circ}F$, 1/2 hour; WQ
2. $1050^{\circ}F$, 1/2 hour; cool to $510^{\circ}F$ at $19^{\circ}F$/hour.

One half of the specimens were precracked following heat treatment and all were broken in impact at test temperatures of $+80^{\circ}F$ and $-40^{\circ}F$.

C. Results

Figure 6 compares the resultant values of $(W/A)_{PCI}$ for each steel with the corresponding results for the as-received gun tubes. Hardness measurements of all specimens indicate that neither heat treatment (a) nor (b) caused any measurable change in hardness from the as-received condition. Thus, any increases in toughness due to reheating are not associated with additional tempering.

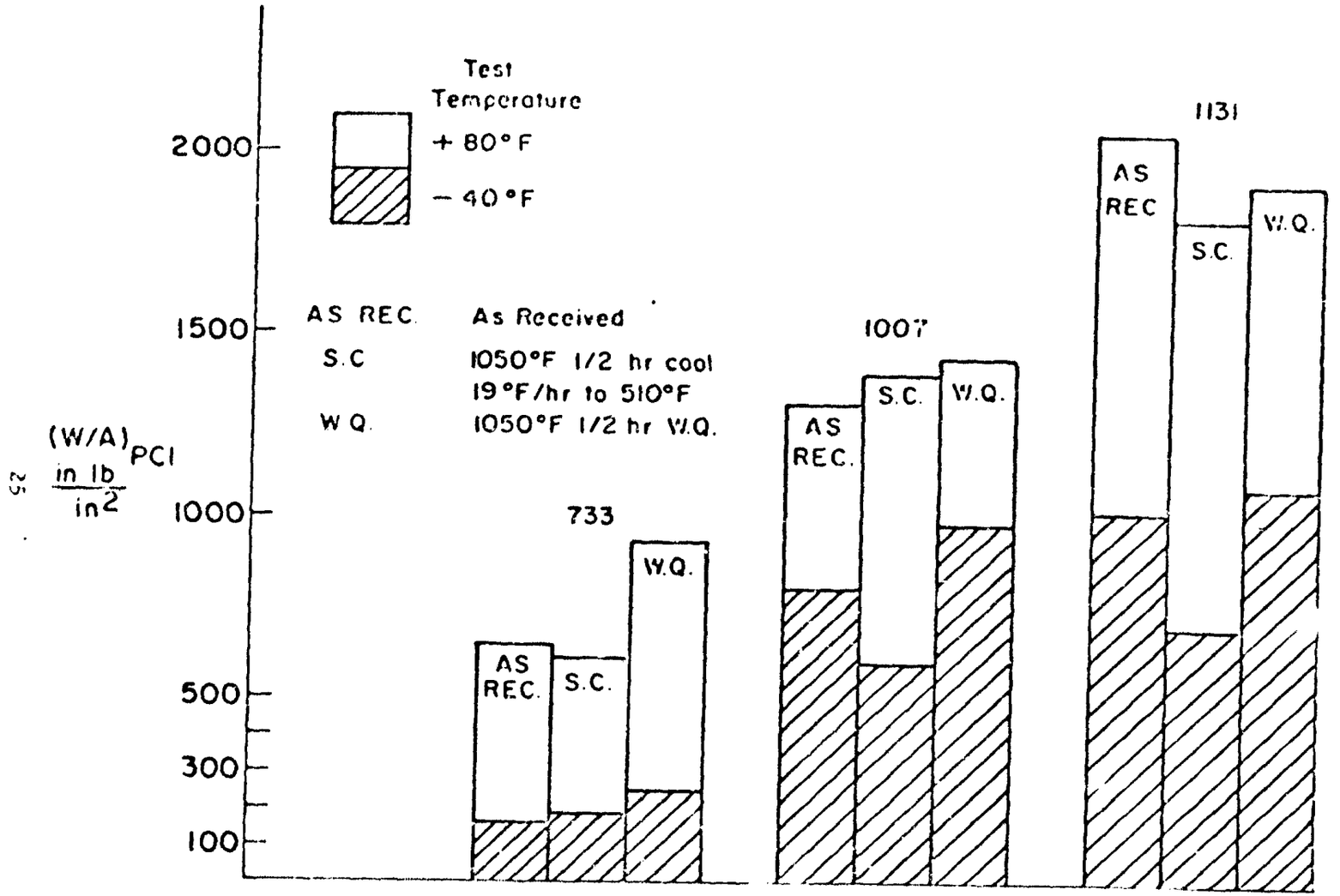

Figure 6. Temper Embrittlement Testing of Program Steels.

The criteria used for judging whether or not a tube is temper embrittled relies on a comparison of $(W/A)_{PCI}$ at $-40^{\circ}F$ among the as-received, slow cooled and water quenched conditions. $(W/A)_{PCI}$ at $+80^{\circ}F$ may or may not indicate the presence of temper embrittlement.

Based on this criteria, it is evident that all three tubes are susceptible to temper embrittlement. In addition, the following observations can be made.

Tube No. 733 The correspondingly low values of $(W/A)_{PCI}$ at $-40^{\circ}F$ and $+80^{\circ}F$ for the as-received and slow cooled conditions as compared to the water quenched condition indicate that tube no. 733 was temper embrittled during production.

Tube No. 1007 $(W/A)_{PCI}$ (at $-40^{\circ}F$) for the as-received tube is intermediate between $(W/A)_{PCI}$ for the quenched and the slow cooled conditions. Evidently, tube no. 1007 has suffered temper embrittlement during production to a lesser degree than in the case of tube no. 733.

Tube No. 1131 The correspondence of $(W/A)_{PCI}$ at $-40^{\circ}F$ for the as-received condition and the quenched condition as compared to the slow cooled condition suggests that, although tube no. 1131 is susceptible to temper embrittlement, it was not adversely effected during production.

It should be noted that even in the quenched condition, the order of increasing $(W/A)_{PCI}$ is still tubes no. 733, 1007, 1131.

The following may be listed as possible causes for the observed embrittlement.

1. Tempering of tube no. 733 for a long period at $960^{\circ}F$. The temperature for the maximum rate of temper embrittlement at constant temperature seems to lie close to $950^{\circ}F$ for low alloy (< 5% total alloying elements) steels (2).

2. The presence of more Cr in tube no.733 as compared to tubes no.1007 and 1131. Cr increases the susceptibility to temper embrittlement (3).

3. The presence of Mn above .6% in tube no.733. Mn additions below .6 to .7% seem to have little effect on temper embrittlement. The presence of Cr intensifies the embrittling effect of Mn (2).

Recent studies (4,5) indicate that the presence of traces of Sb, Sn, As and P are important in causing susceptibility to temper embrittlement. Without a more detailed study, no positive conclusions may be drawn about the true cause of the observed temper embrittlement.

D. Crack Propagation Energy

Values of $(W/A)_{CI}$ corresponding to each steel, heat treatment and test temperature are shown in Figure 7; also included for comparison are the values of $(W/A)_{PCI}$ from Figure 6. The -40°F Charpy impact energies generally reflect the same states of temper embrittlement that the -40°F PCI testing revealed.

Table 9 lists the ratio $(W/A)_{PCI}/(W/A)_{CI}$ for the data shown in Figure 7. $(W/A)_{PCI}/(W/A)_{CI}$ represents that percentage of energy in a standard Charpy impact test available to resist crack extension after a crack has been initiated. It is important to note that in the water quenched condition, tube no.733 almost achieves the required 10 ft/lbs at -40°F. However, only 30% of this energy is available to resist crack extension. Corresponding values of $(W/A)_{PCI}/(W/A)_{CI}$ are 50% and 78% for tubes no.1131 and 1007, respectively. This raises some question about the validity of a criterion specifying a minimum Charpy impact energy for structures assumed to contain cracks at early stages of service.

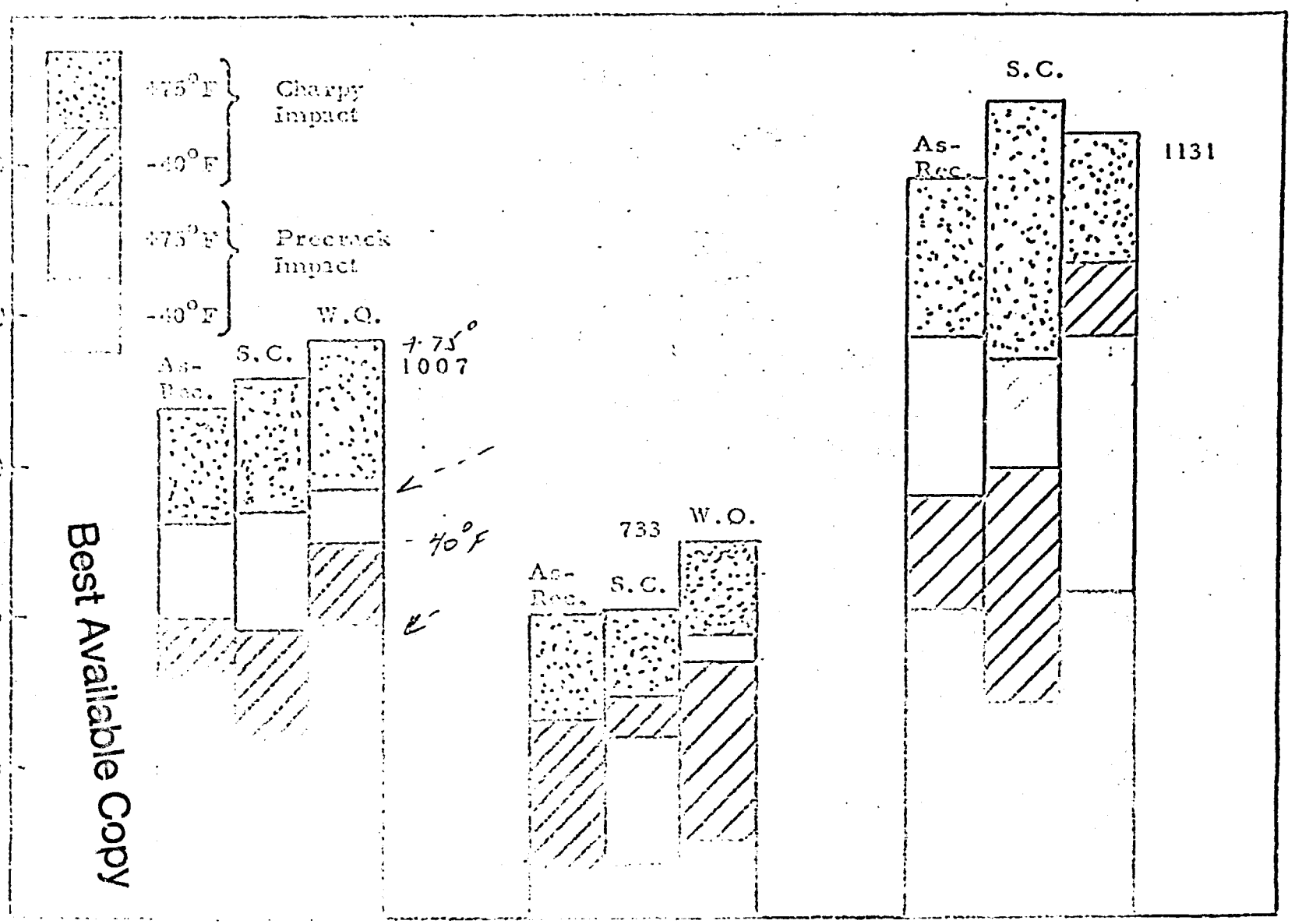

...ations in Tables 1131, 1007 and 733. As-Received Indicates Production Heat Treated ... S.C. Indicates Reheating to 1050°F 1/2 Hour and Cooling 19°F/Hour to 510°F W.Q. ...ling to 1050°F for 1/2 Hour and Water Quenching.

TABLE 9

EFFECT OF TEMPER EMBRITTLEMENT

ON CRACK PROPAGATION ENERGY

Steel No.	Heat Treatment	Test Temp °F	$(W/A)_{PCI}/(W/A)_{CI}$ %
733	SC	-40	25.6
		+75	59.1
	WQ	-40	30.1
		+75	76.4
	As-Received	-40	25.5
		+75	63.3
1007	SC	-40	61.2
		+75	76.9
	WQ	-40	78.4
		+75	74.3
	As-Received	-40	80.3
		+75	77.5
1131	SC	-40	46.9
		+75	67.4
	WQ	-40	50.0
		+75	71.2
	As-Received	-40	72.2
		+75	84.2

VI. HIGH STRESS, LOW CYCLE FATIGUE TESTS

A. Fatigue Testing Apparatus

In order to carry out high stress, low cycle fatigue tests, a Sonntag SI-10R rotating beam fatigue machine was modified as shown in Figure 8. In carrying out such a fatigue test, a precracked specimen (of the design shown in Figure 1b) was held horizontally in an inverted anvil with the V-notch facing upward. Cyclic bending of the specimen was accomplished by a cam driven by a constant speed electric motor (120 rpm). Contact with the specimen was made with a ball bearing attached to the cam with the outer race free to rotate. The cam was mounted on a shaft which was offset about 1/16 inch from the axis of rotation. Maximum bend deflections up to about 0.010 inch for a 1.75 inch span distance were obtained by moving the anvil in a vertical direction either toward or away from the cam axis. A rack pinion type dial indicator with an accuracy of $\pm$ 0.0001 inch was used to measure bend deflections.

B. Fatigue Testing Procedure

In order to run a fatigue test at a selected initial nominal stress level, the required load (P) can be calculated from Eq. (2). The bend delfection, y, necessary to attain the required load is given by the elastic beam relation:

$$y = \frac{PL^3}{4EB(w-a_o)^3} \qquad (2)$$

where E is Young's modulus for steel (30×10^6 psi).

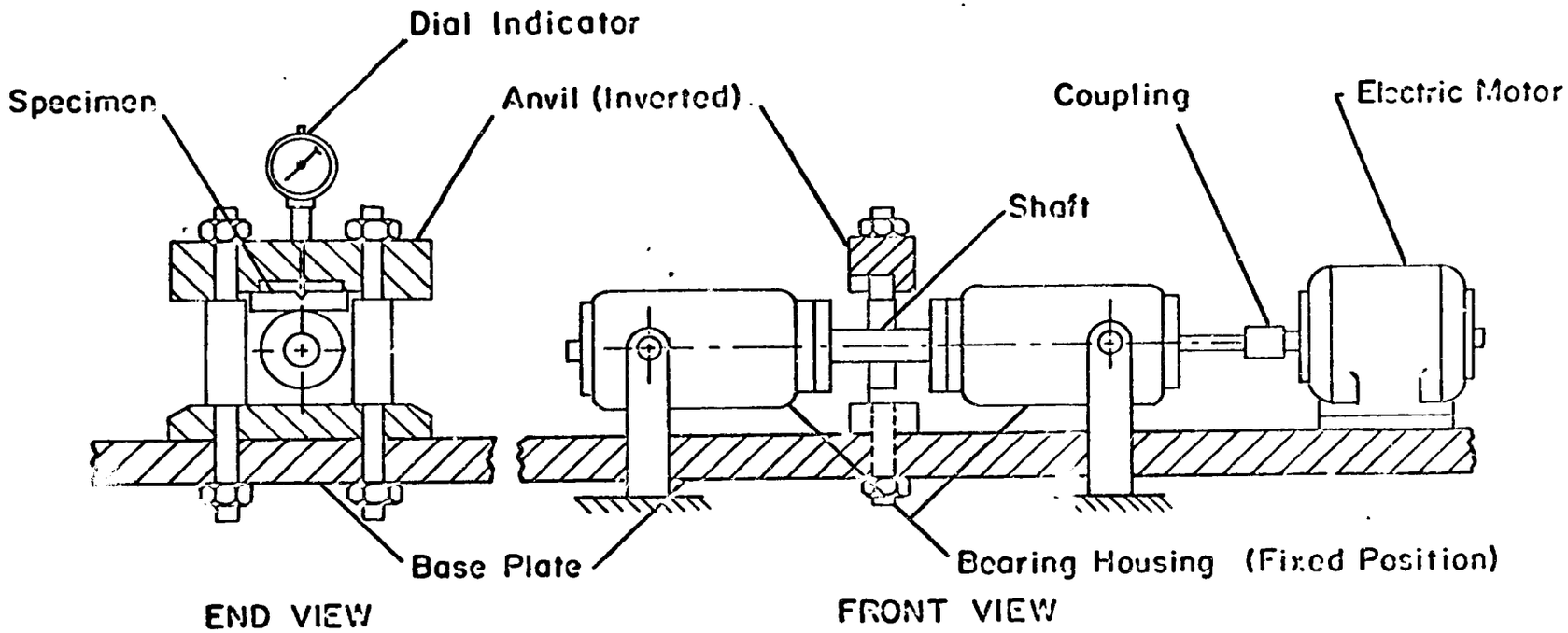

Figure 8. High Stress Low Cycle Fatigue Testing Machine for Applying an Alternating Deflection (Zero to Constant Maximum) and Achieving an Alternating Tensile Stress at the Crack Tip of a Precracked Bend Specimen Subjected to 120 RPM.

The nominal stress at the root of the crack is given by:

$$\sigma_{nom} = \frac{3PL}{B(w-a)^2} \tag{3}$$

By combining Eqs. (2) and (3), σ_{nom} may be expressed as function of y and a as follows:

$$\sigma_{nom} = \frac{12\, y\, E\, (w-a)}{L^2} \tag{4}$$

The procedure used in carrying out the high stress, low cycle fatigue tests was as follows: (a) precrack heat treated bend specimens to a depth of about 30 mils, (b) heat tint precrack fatigue zone at 500°F, (c) conduct low cycle high stress fatigue tests at the selected initial σ_{nom} level for a total of 1200 cycles at 120 rpm in argon or distilled water, (d) break specimen in impact to expose fatigue zones, (e) measure the depth over which the low cycle fatigue occurred and (e) calculate the average rate of fatigue crack growth (expressed as inch/cycle).

C. Results

Figures 9 through 13 show the variation of average crack growth rate $(\frac{\Delta a}{\Delta N})_{ave}$ with nominal stress, σ_{nom} in argon and water for the five program steels.

The effect of distilled water on $(\frac{\Delta a}{\Delta N})_{ave}$ is apparent when the data for the three gun tubes (Figures 9, 10 and 11) is examined. However, fatigue crack growth in the Marage 250, Figure 12 and HP-9-4-30, Figure 13, seems to be insensitive to those environments investigated.

For purposes of comparison, this data is shown in Figure 14 as $(\frac{\Delta a}{\Delta N})_{ave}$ vs. $\frac{\sigma_{ave}}{\sigma_{ys}}$, where σ_{ys} is taken as the .1% offset yield strength for each steel.

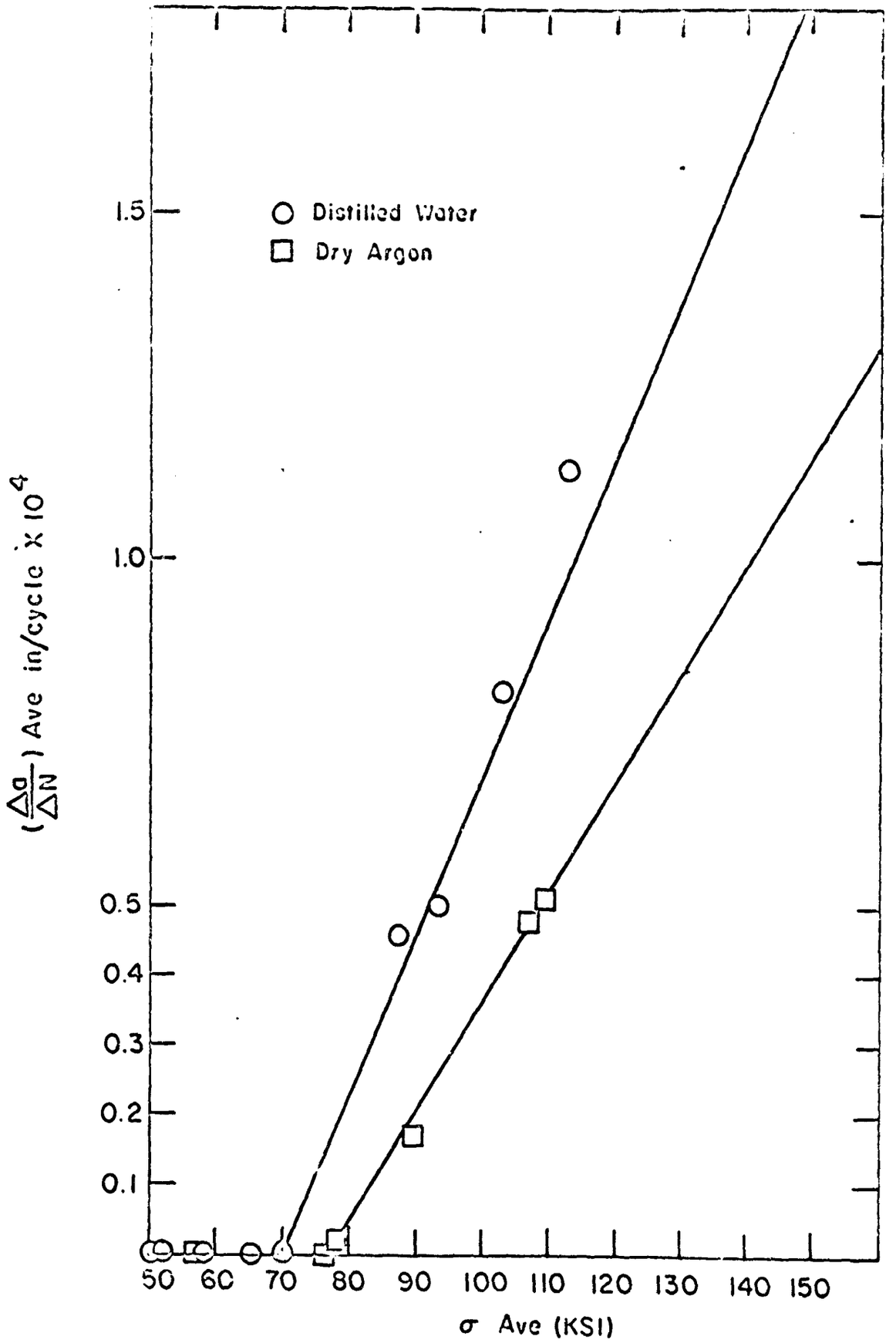

Figure 9. Plots of Average Rate of Fatigue Crack Growth $(\Delta a/\Delta N)_{ave}$, vs. Average Nominal Stress at Crack Tip, σ_{ave}, for Tube No. 1131 Tested in Distilled Water and Dry Argon Environments.

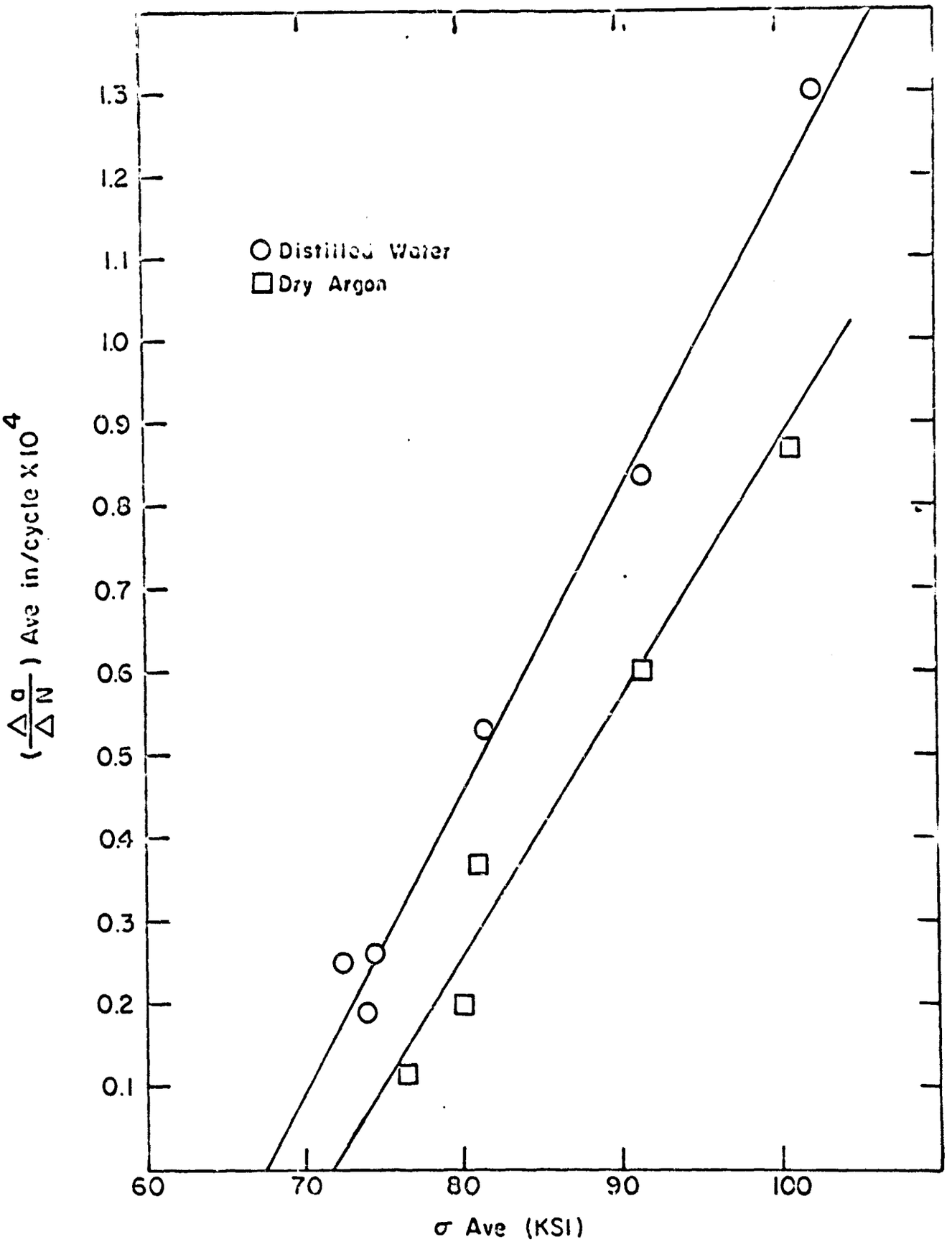

Figure 10. Plots of Average Rate of Fatigue Crack Growth, $(\frac{\Delta a}{\Delta N})_{ave}$, vs. Average Nominal Stress at Crack Tip, σ_{ave}, for Tube No. 1007 Tested in Distilled Water and Dry Argon Environments.

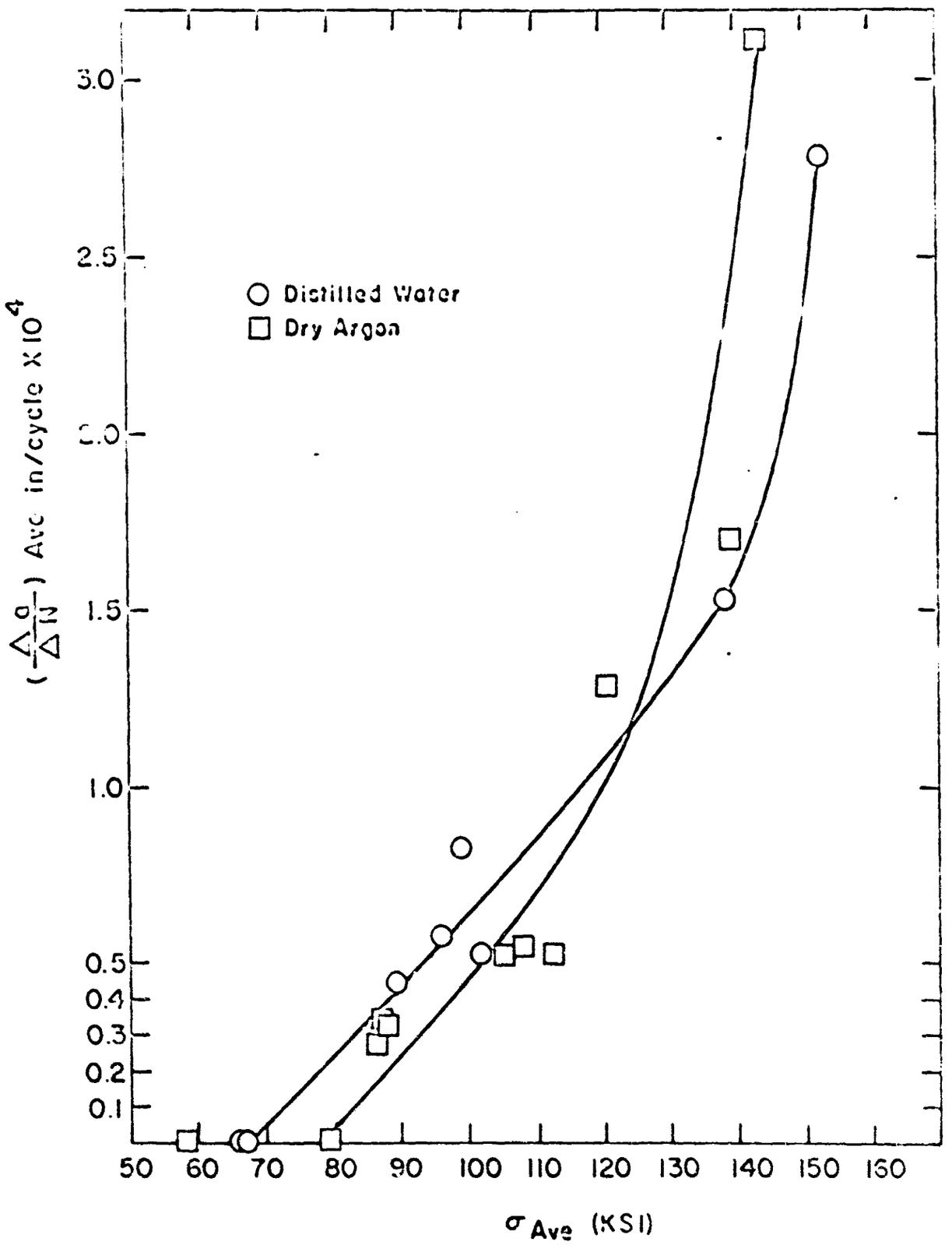

Figure 11. Plots of Average Rate of Fatigue Crack Growth, $\left(\frac{\Delta a}{\Delta N}\right)_{ave}$, vs. Average Nominal Stress at Crack Tip, σ_{ave}, for Tube No. 733 in Distilled Water and Dry Argon Environments.

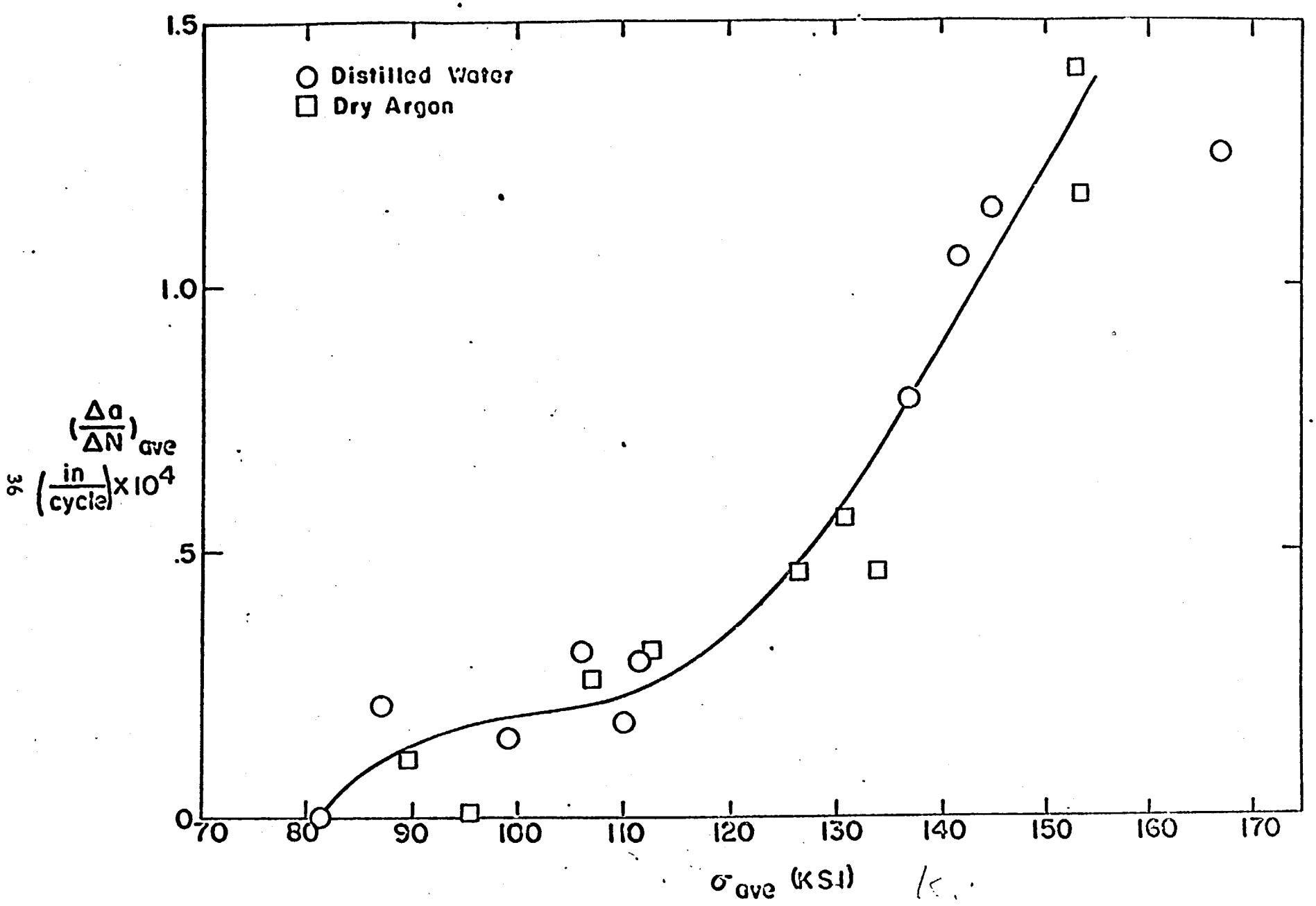

Figure 12. Low Cycle, High Stress Fatigue of Marage 250 in Dry Argon and Distilled Water.

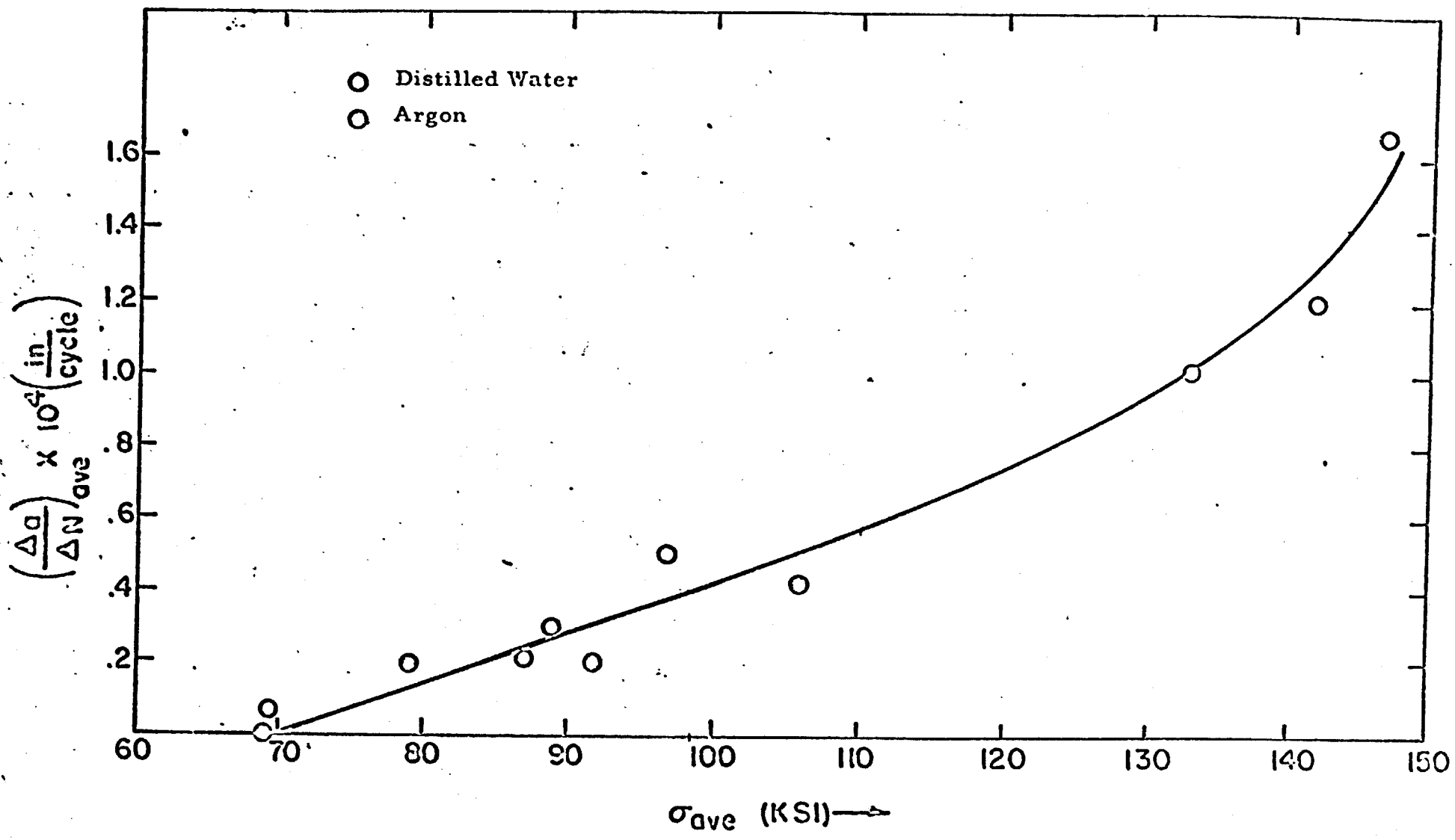

Figure 13. Low Cycle, High Stress Fatigue of Republic 9-4-30 in Dry Argon and Distilled Water.

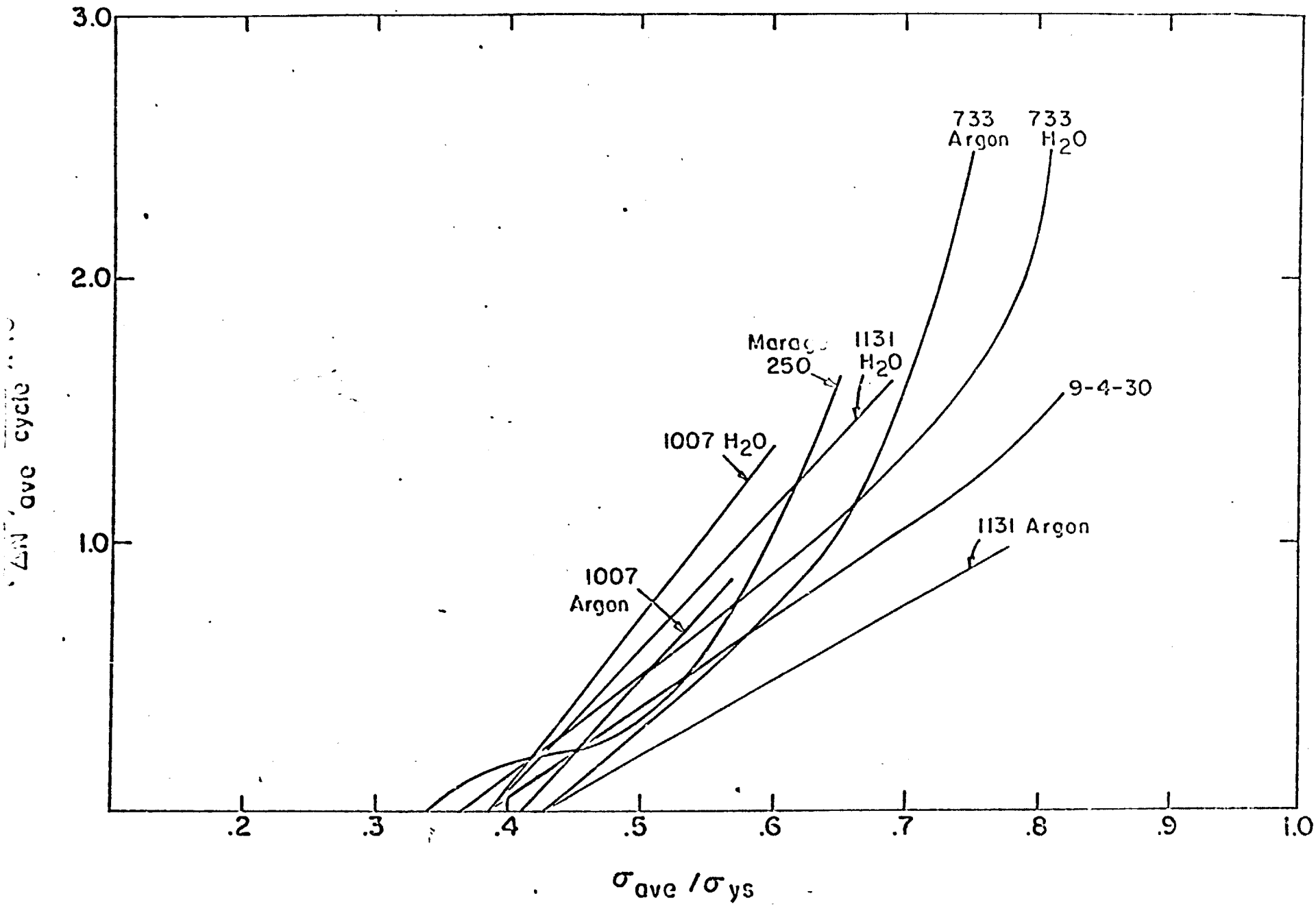

Figure 14. Low Cycle, High Stress Fatigue of Tubes No. 1007, 1131, 733, 9-4-30 and the Marage 250 Steel in Dry Argon and Water.

In all but the maraging steel, the initial ($\sigma_{ave}/\sigma_{ys} < .6$) relationships between $(\Delta a/\Delta N)_{ave}$ and $(\sigma_{ave}/\sigma_{ys})$ were found to be linear. For $\sigma_{ave}/\sigma_{ys} > .6$, tube no. 733 shows a nonlinear dependence of $(\Delta a/\Delta N)_{ave}$ on σ_{ave}/σ_{ys} while the other steels exhibit a straight line dependence.

At the present time, it is not felt that any particular emphasis can be placed on minor variations in slope, although differences such as those between 9-4-30 and the Marage 250 are meaningful.

Of more interest at the present time is the lowest value of $\frac{\sigma_{ave}}{\sigma_{ys}}$ at which measurable fatigue crack growth occurs in 1200 cycles. This is a basis for comparison of the fatigue resistance of the program steels. These values are given below in Table 10.

TABLE 10

STRESS LEVEL FOR INCEPTION OF CRACK GROWTH

Steel	Environment	$\frac{\sigma_{ave}}{\sigma_{ys}}$ at $(\frac{\Delta a}{\Delta N}) = 0$
Marage 250	Argon and water	0.340
733	Water	0.365
1007	Water	0.385
1131	Water	0.385
9-4-30	Argon and water	0.385
1007	Argon	0.410
733	Argon	0.425
1131	Argon	0.425

It can be seen that the behavior of the gun steels in water correlates well with service behavior and with comparisons on the basis of fracture toughness parameters.

Although crack propagation (in 1200 cycles) was found to occur at low stress levels in these steels, other investigators have encountered similar behavior in Ti-8Al-1Mo-1V and AM-350 stainless steel during fatigue cracking studies not involving crack initiation (6).

D. Electron Fractography

PSB specimens of tubes no. 733, 1131 and 1007 were cycled in dry argon as described in Section VIA. After cycling, the specimens were broken in impact and the fracture surfaces were replicated (7).

The fracture surfaces at 4300X for tubes 1131, 733 and 1007 were similar in appearance. Figure 15 shows typical fractographs obtained on tube no. 1131. The crack growth rate, as computed from measurement of the fractographs, was found to agree favorably with $(\Delta a/\Delta N)_{ave}$ which was measured in the low cycle fatigue tests. This correlation breaks down near the end of the fatigue crack, where the crack growth rate increases rapidly.

It is of interest to note that in Figure 15 the crack growth rate is increasing, while the nominal stress level is decreasing slightly.

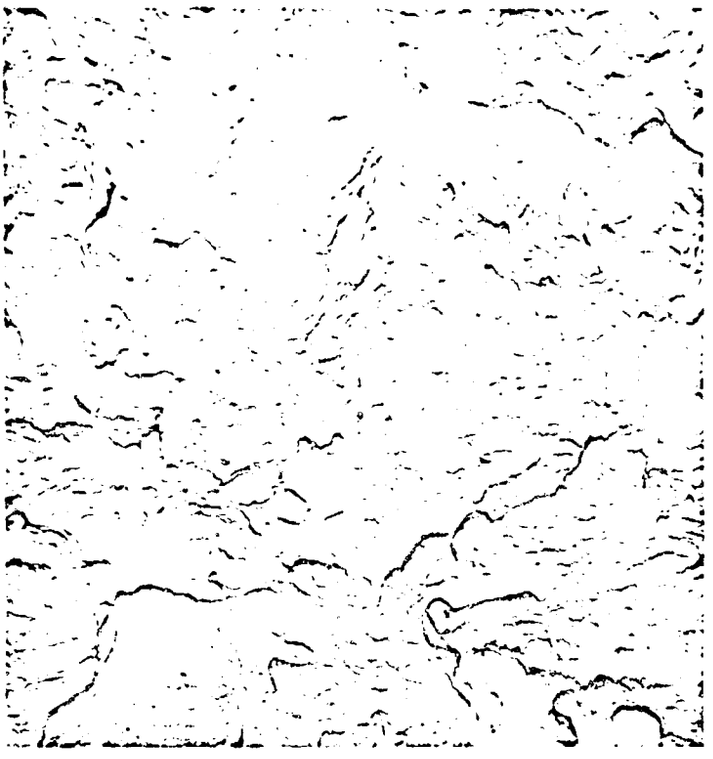

a) σ_{nom} = 124 ksi, beginning of test

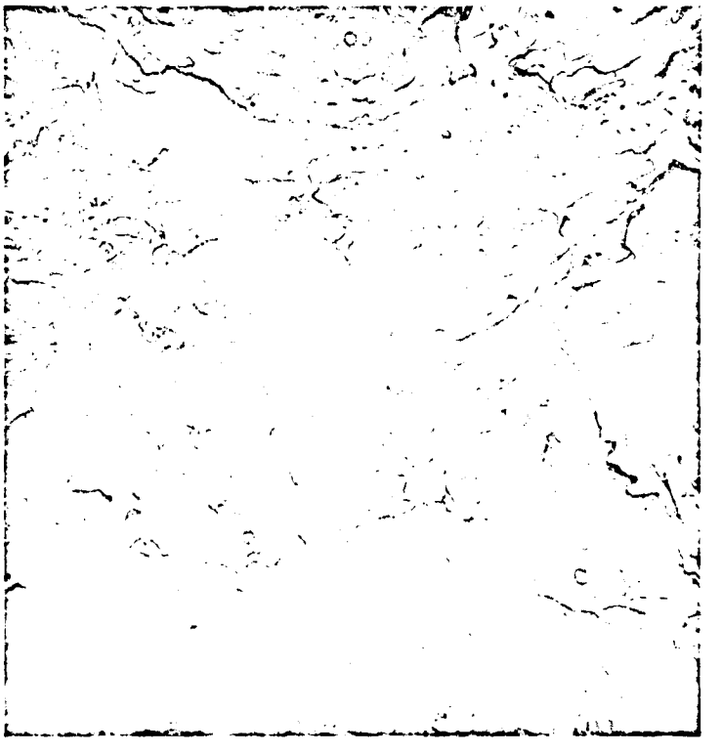

b) σ_{nom} = 119.9 ksi, end of test

Figure 15. Tube No. 1131 in Dry Argon at σ_{ave} = 121.9 ksi 4300X.

VII. STRESS CORROSION CRACKING TESTS

A. Modified Brown Stress Corrosion Testing Procedure

A modification of the Brown (8) apparatus was constructed to expedite carrying out relatively long time stress corrosion tests at constant load. As shown in Figure 16, this apparatus utilizes a cantilever beam loading system with a mechanical advantage of 10:1. This system was designed to apply a constant bending moment to the specimen throughout the test. For smooth loading of the specimen, the weights were lowered on to the loading platform by means of a hydraulic jack.

In carrying out a test, a precracked face-notched bend specimen was clamped to the base plate in a horizontal position with the V-notch facing upwards. A corrodent cell made of polyurethane filled with distilled water was positioned to surround the central portion of the specimen. With the exception of the V-notch, this region was coated with lacquer for a distance equal to the effective length of the cell.

During the course of a stress corrosion test, the deflection of the specimen was continually measured by means of a rack and pinion type dial indicator mounted collinear with the anvil.

B. Results

Initial applied stress intensity and time to failure were obtained and are shown in Figures 17, 18 and 19.

The data is functionally similar to that found for 4340 by Brown (8), but different than that found by Steigerwald (9). The differences between the latter apparently were related to incubation time for film formation; once crack growth was initiated, however, the functional dependence of failure time on initial applied stress intensity become quite similar.

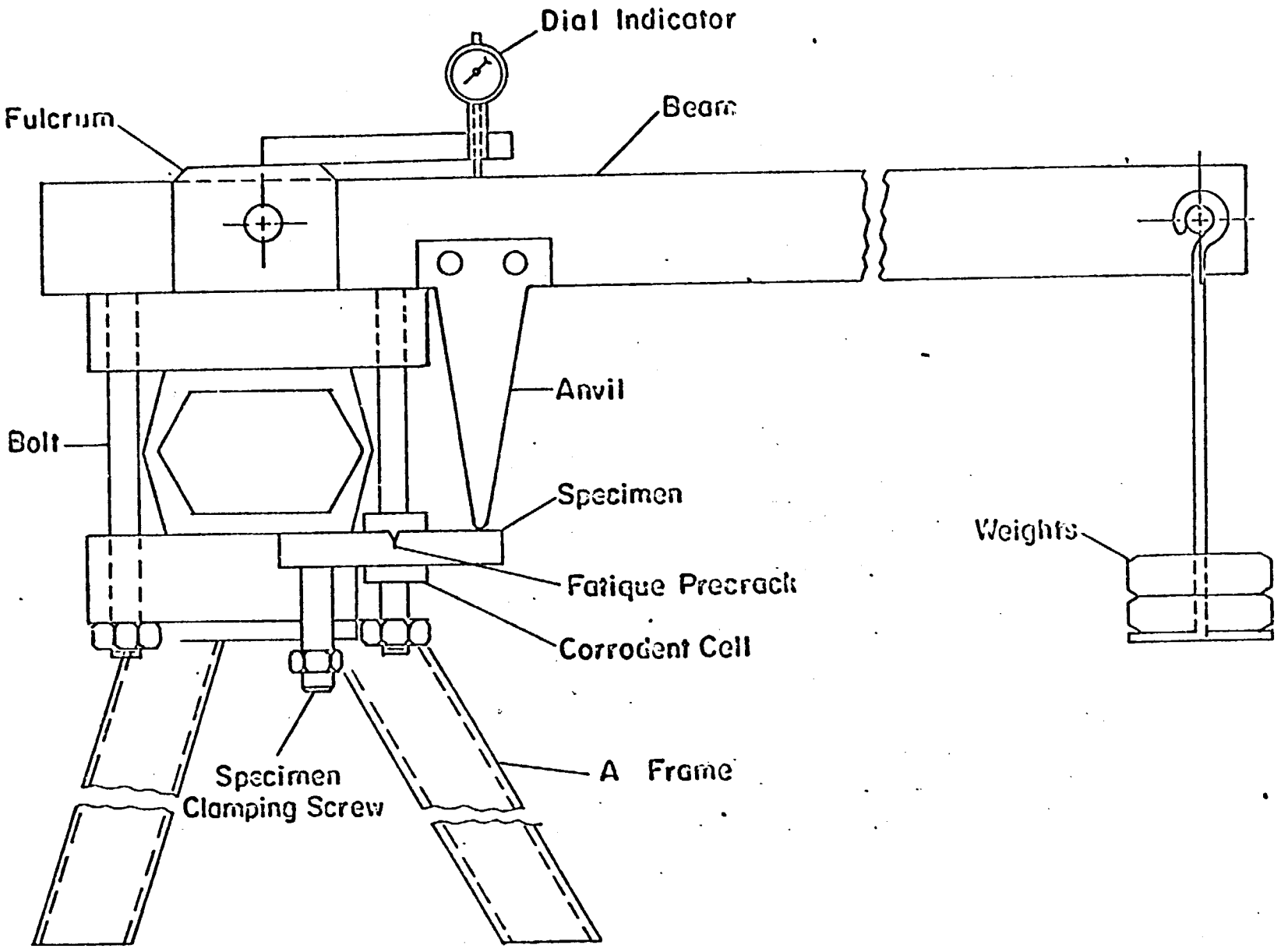

Figure 16. Modified Brown Cantilever Beam Apparatus for Determining Stress Corrosion Cracking Susceptibility.

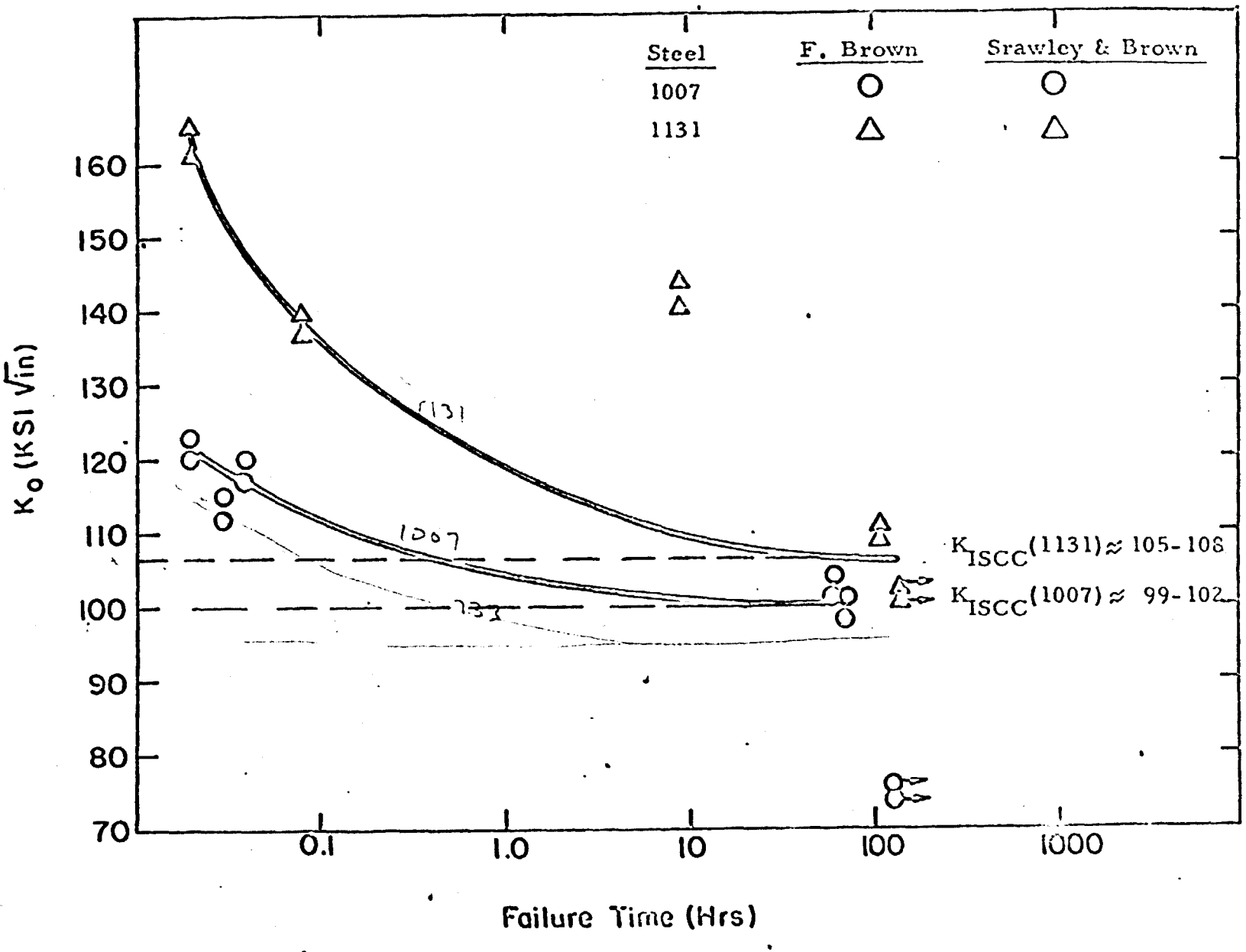

Figure 17. Stress Corrosion Cracking of Steels 1131 and 1007.

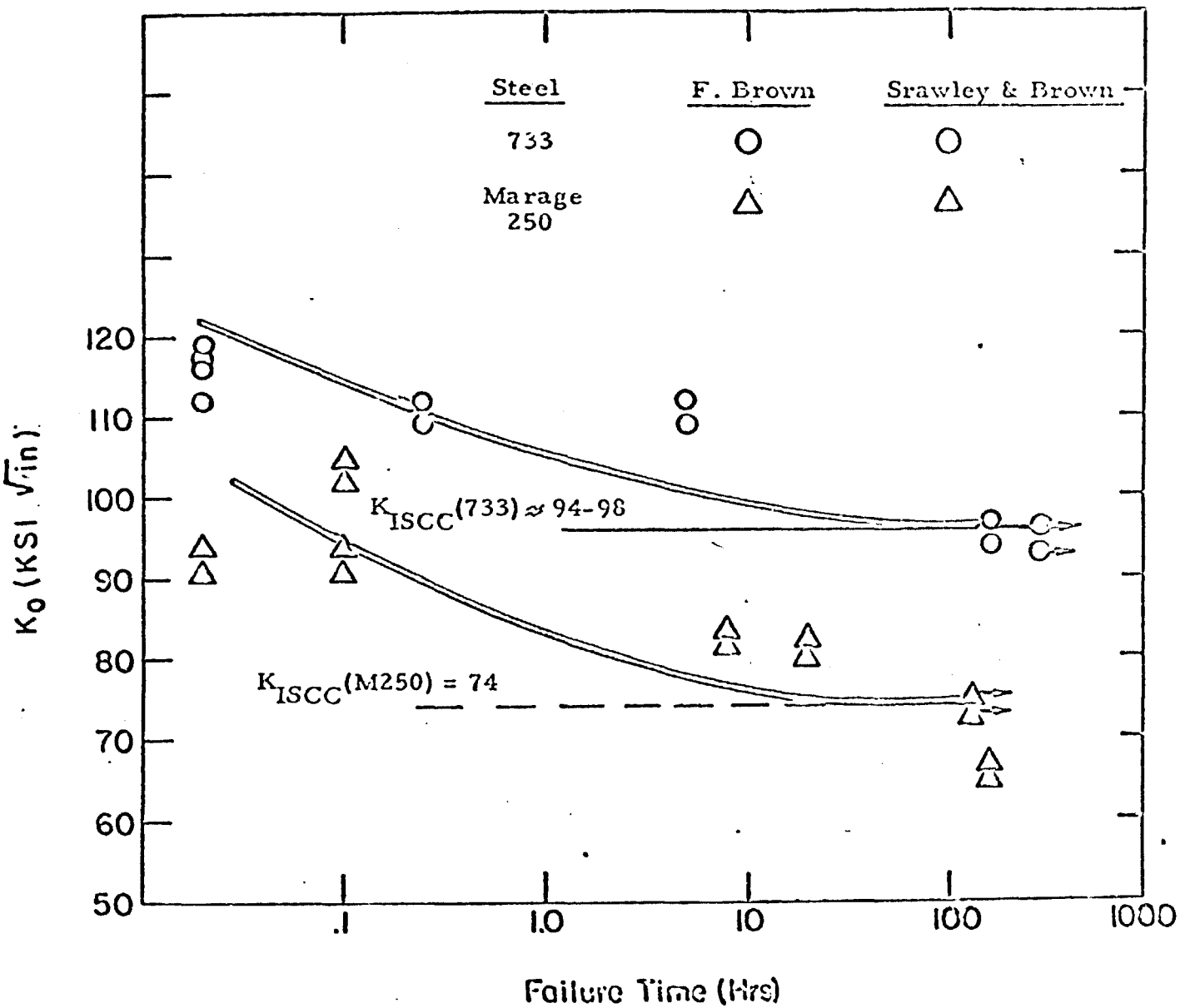

Figure 18. Stress Corrosion Cracking of Steels M250 and 733.

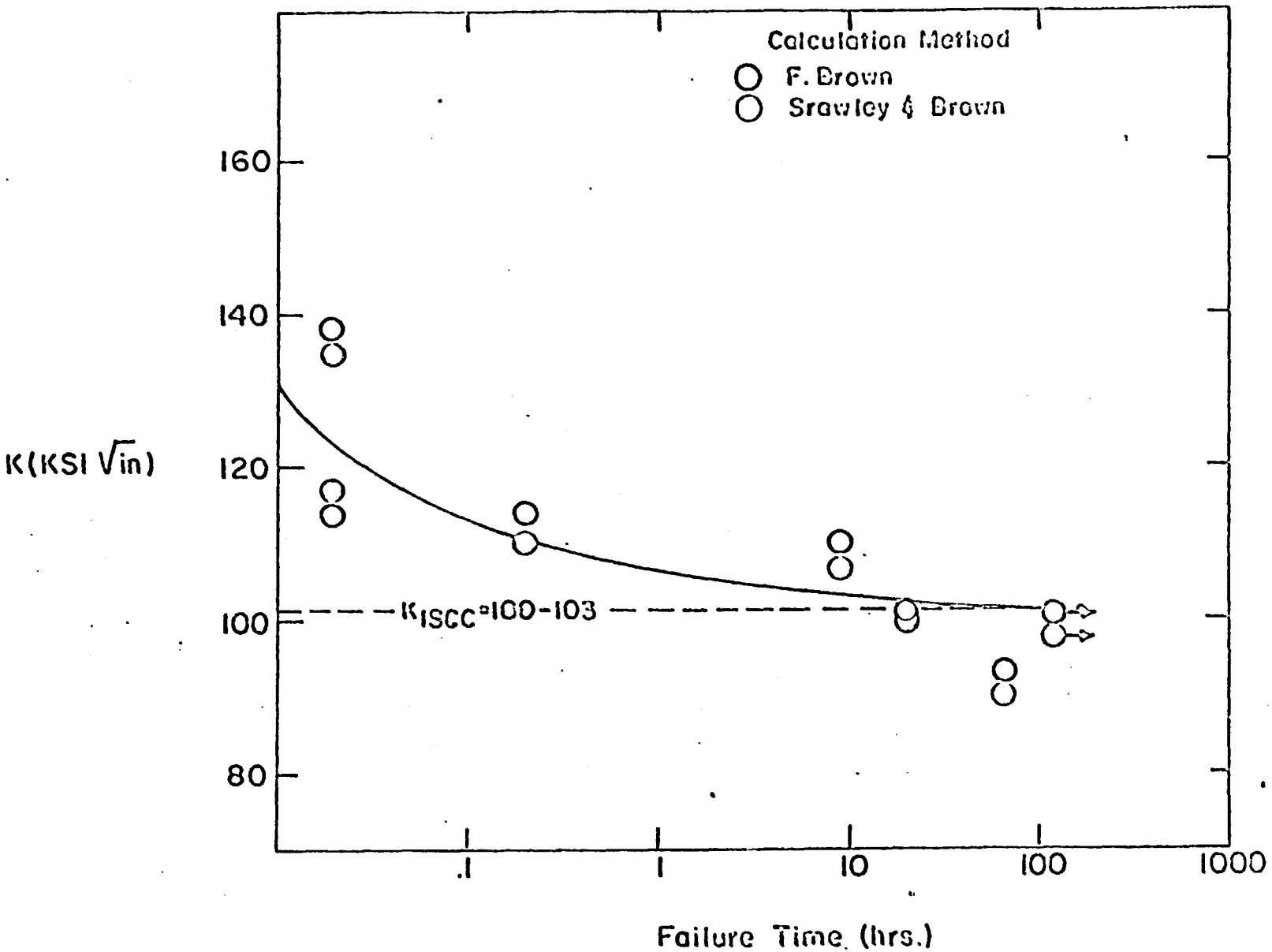

Figure 19. Stress Corrosion Cracking of Republic 9-4-30.

The initial applied stress intensity below which no failure occurs in approximately 300 hours was designated K_{ISCC}. The values of K_{ISCC} for the program steels are given in Table 11 in increasing order.

TABLE 11

BROWN STRESS CORROSION CRACKING TESTS

Steel	K_{ISCC} ksi $\sqrt{in}$
Marage 250	74
733	94-98
1007	99-102
9-4-30	100-103
1131	105-108

It can be seen that the values of K_{ISCC} correlate well with both fracture toughness data and service behavior. It also is of particular interest to note the poor behavior of the Maraging steel. Emphasis should again be placed on the fact that subsized specimens were used; the data is presented for purposes of comparisons in this program and should not be used for comparison with data for larger specimen sizes.

C. Electrical Potential Measuring Equipment

The equipment constructed for measuring crack growth by means of change in electrical potential is schematically illustrated in Figure 20. Following the method of Anctil (10), an aluminum foil calibration specimen with length and width dimensions about fifteen times those of a bend specimen was used. This specimen was subjected to simulated crack extension by cutting with a razor blade in the width direction starting from the root of the notch. Maintaining a constant

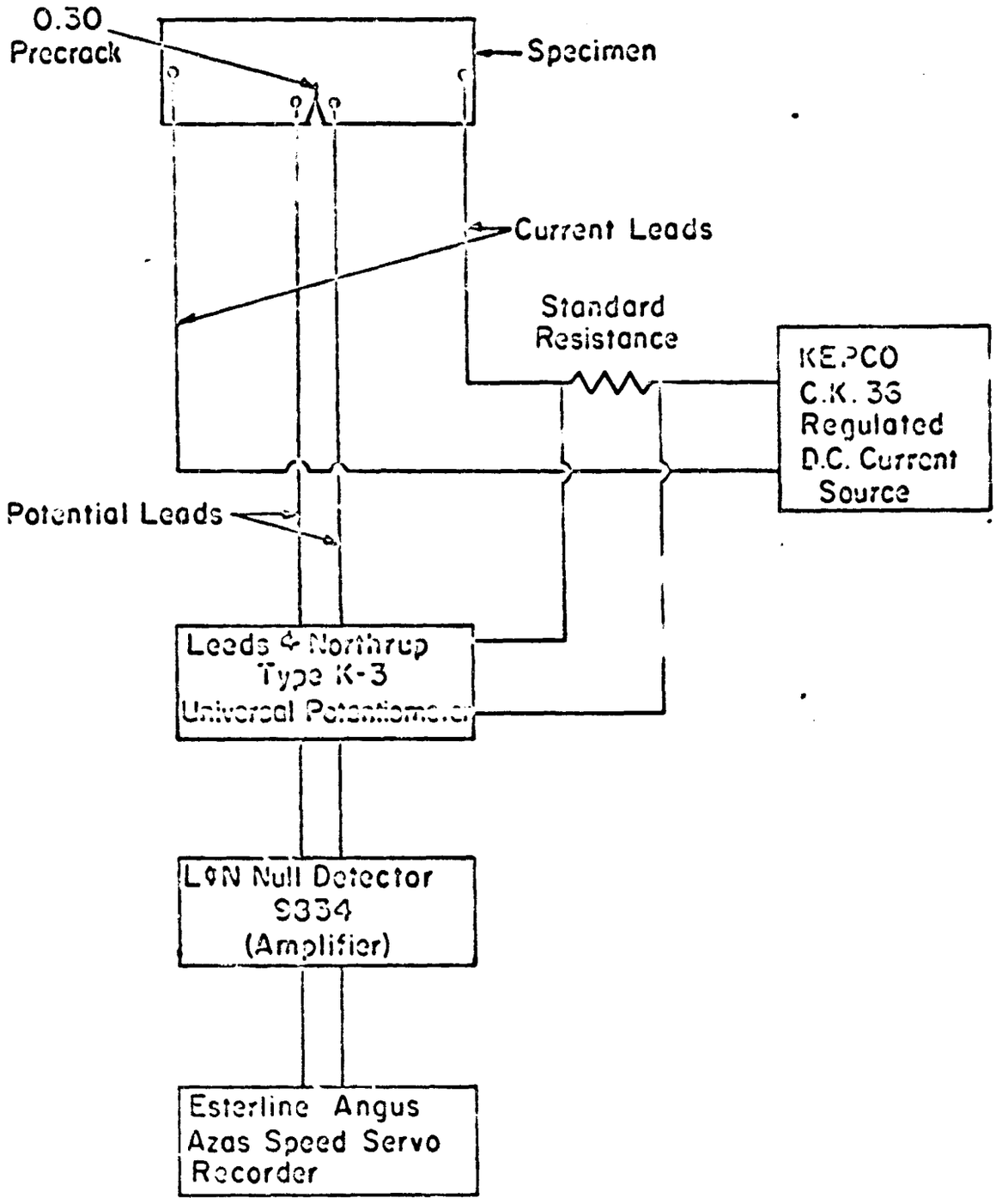

Figure 0. Schematic Diagram of Electrical Potential Apparatus for Measuring Crack Extension.

current of one amp, the voltage drop across the potential leads was measured as a function of crack extension. The crack lengths were measured optically with a magnifier lens.

In Figure 21, the potential drop V is plotted as a dimensionless ordinate quantity V/V_o where V_o is the potential drop corresponding to the initial precrack a_o. Similarly, the crack length a is plotted as a dimensionless abscissa quantity a/a_o. The resulting family of curves shown in Figure 21 are used to obtain crack extension from changes in potential as measured during stress corrosion and slow bend tests.

D. Electrical Potential Measurements of Slow Crack Growth in Stress Corrosion Cracking

PSB specimens of tubes no. 733 and 1007 (oriented so that crack growth is in the radial direction) were prepared for crack length measurements by spot welding leads on either side of the precrack immediately adjacent to the root of the crack. Current leads were affixed in the same manner to the ends of the specimen along the center line.

The specimens were inserted in a ManLabs SB-750 slow bend machine and distilled water was placed in the notch. After the appropriate connections to the electrical potential measuring apparatus were made, the specimens were loaded to a desired stress level and held at constant deflection. The distilled water in the notch was replenished as the test proceeded. Both bending load and potential drop at 1 ampere current flow were recorded as a function of time until the specimen either fractured or crack growth ceased.

After the test was stopped, the specimen was broken in impact to reveal the precrack depth a_o. Using the calibration data in Figure 21, the precrack depth

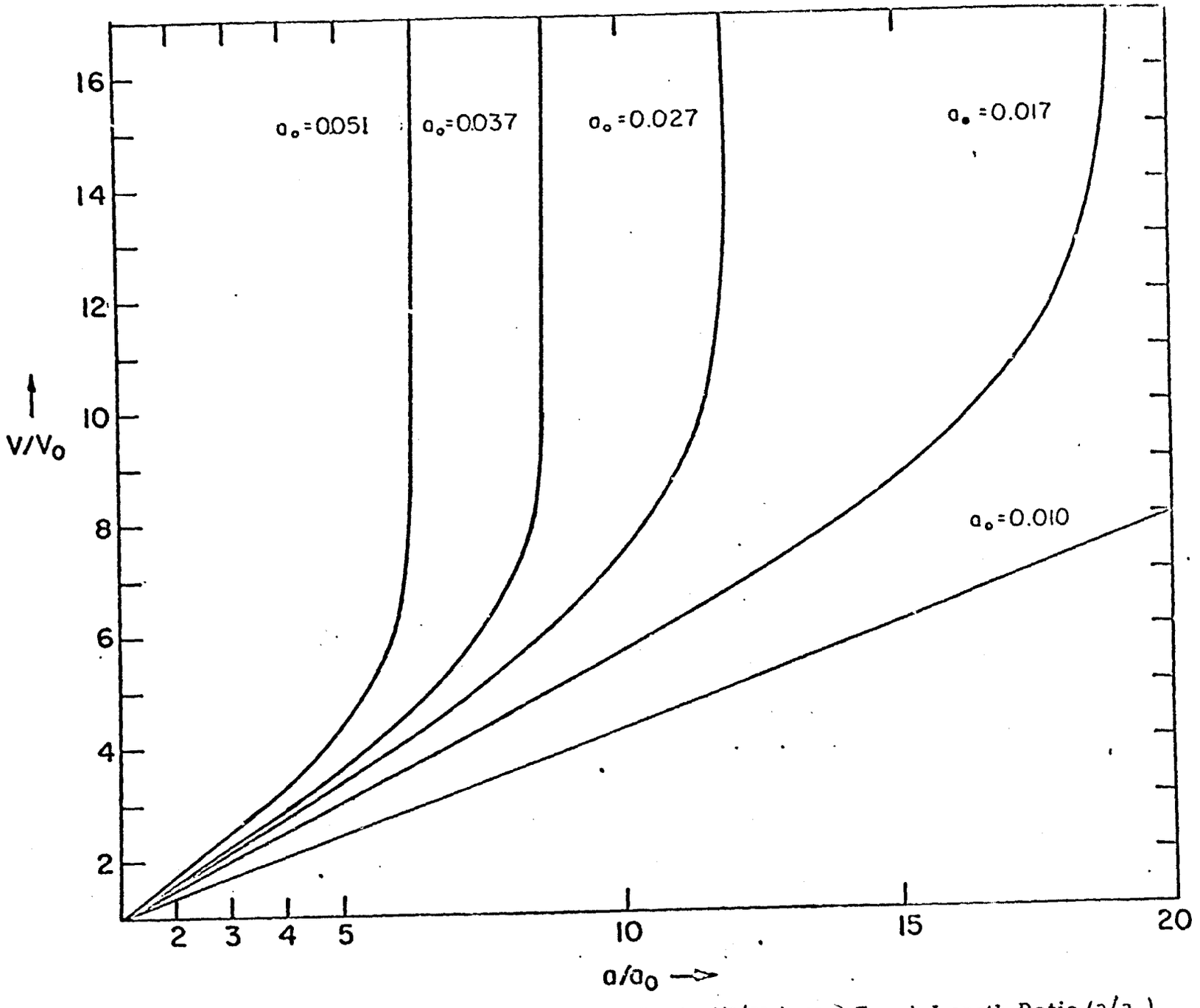

Figure 21. Calibration of Potential Change Ratio (V/V_o) vs. Crack Length Ratio (a/a_o) for Various Initial Crack Lengths (a_o).

and the recorded values of change of potential drop across the crack with time, the crack depth was obtained as a function of time. During the test, at those precrack depths for which calibration data was not available, crack lengths were calculated from the existing calibration data by a six point Lagrangian interpolation using the IBM 1130 computer. When these computed values of crack length were combined with the corresponding recorded values of bending load, the nominal stress at the root of the crack and the applied stress intensity level were obtained as a function of time.

When the change in crack length during the test was normalized to the precrack depth, it was found that the logarithm of this quantity $ln \frac{\Delta a}{a_o}$ was a linear function of time (Figures 22 and 23).

Figure 22 shows the results obtained for tube no.733. The three curves represent the data obtained at three initial stress intensity levels. Each of the plots consist of two straight line segments; the latter segment flattens out as crack growth stops or changes discontinuously as fracture occurs. The gradual tapering off is believed to be associated with geometrical changes in the lead configuration as the load is relieved and also by the departure of the crack front from a straight line. This is further confirmed by the failure of the computed crack depth to agree with the final observed value at crack depths exceeding approximately 0.100 inch.

Since $ln \frac{\Delta a}{a_o}$ is initially proportional to time for all the specimens, the crack depth can be expressed as:

$$ln \frac{\Delta a}{a_o} = mt + B \qquad (5)$$

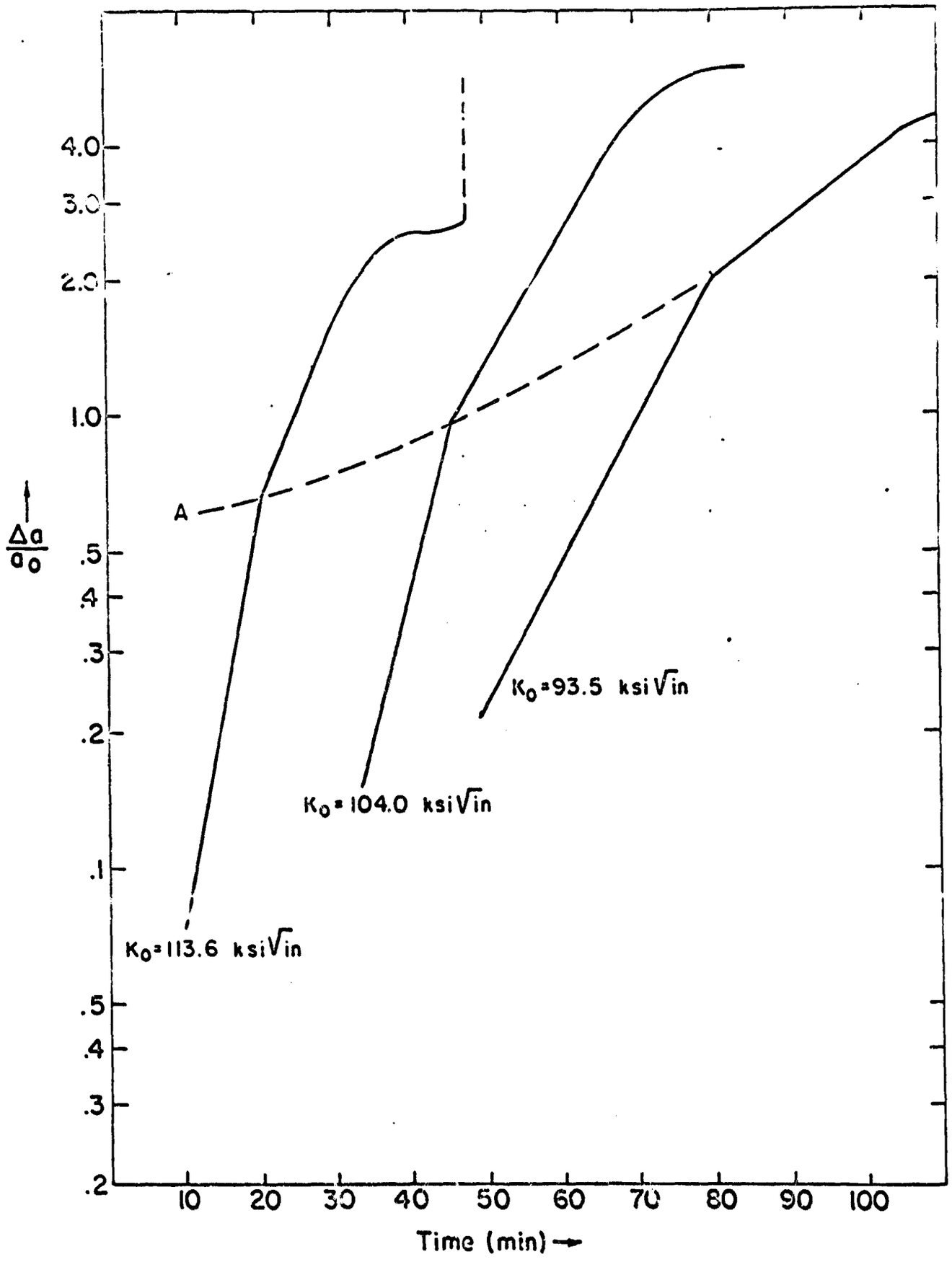

Figure 22. Change in Crack Length During Stress Corrosion Cracking of Tube No. 733 at Constant Deflection.

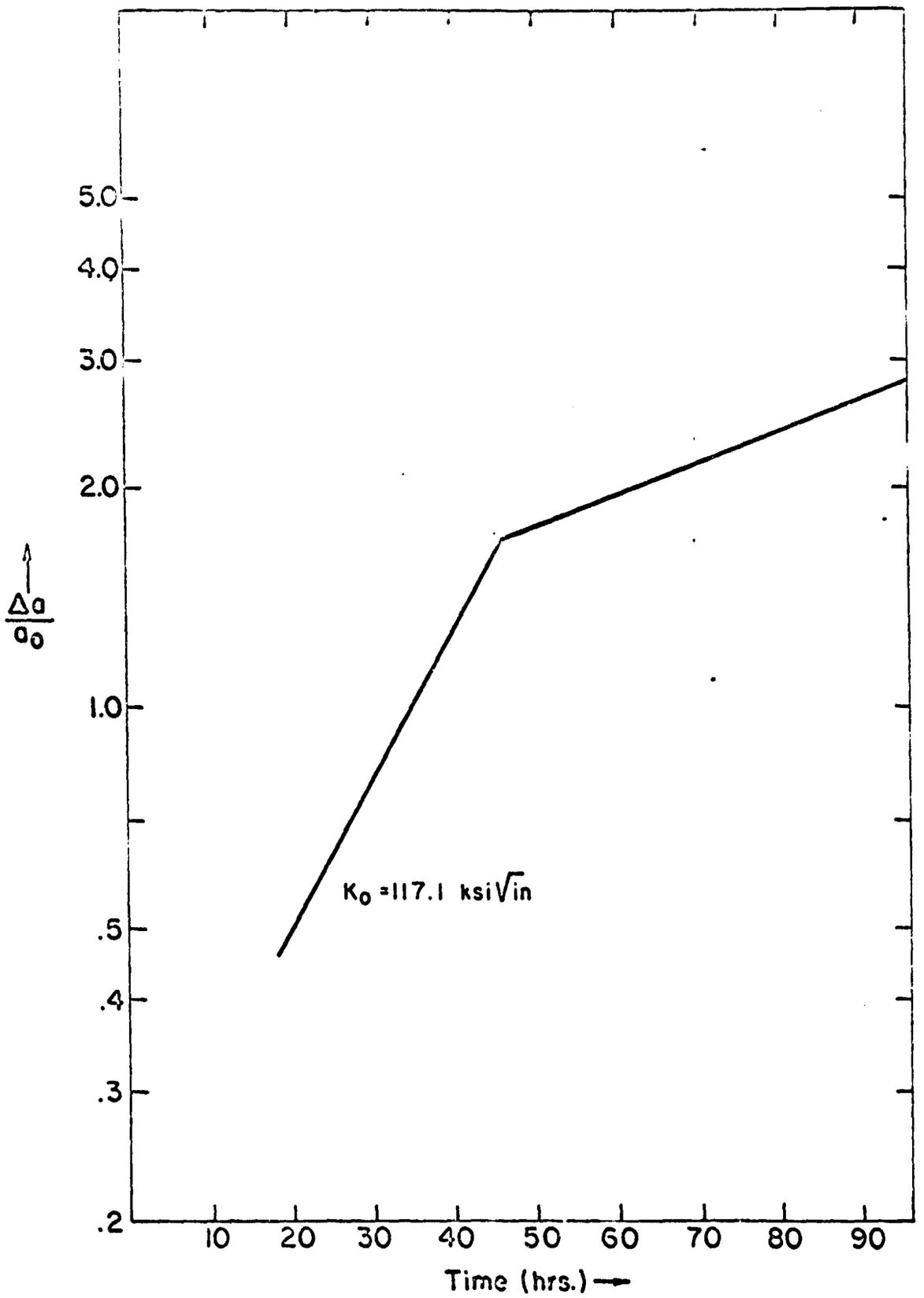

Figure 23. Change in Crack Length During Stress Corrosion Cracking of Tube No. 1007 at Constant Deflection.

where $\Delta a = a - a_o$, m is the slope up to the locus of times marked "A" in Figure 22 and B is the $ln \frac{\Delta a}{a_o}$ intercept at $t = 0$.

Hence, $$a = a_o (1 + e^{mt + B}) \quad (6)$$

and $$\frac{da}{dt} = a_o \; m \; e^{mt + B} \quad (7)$$

When the values of m obtained from Figure 22 are plotted as a function of the initial applied stress intensity K_o a straight line results (Figure 24). Measuring the slope and intercept of this plot shows that:

$$m = \frac{K_o - K'}{133} \quad (8)$$

Where K' is the extrapolated value of K_o at which $m = 0$ (i.e., at which $\frac{da}{dt} = 0$) and is 83.8 ksi $in^{1/2}$ for tube no.733.

Therefore, $$\frac{da}{dt} = a_o \left(\frac{K_o - K'}{133}\right) \; e^{\left(\frac{K_o - K'}{133}\right) t + B} \quad (9)$$

for tube no. 733.

The stress corrosion cracking behavior of tube no. 1007 (Figure 23) is similar to that of tube no.733, except that the test duration is of the order of 100 hours instead of 100 minutes. The value of m is not yet known for tube no. 1007 as only one specimen has been tested. It is interesting to note that the value of K' for tube no.733 is in fair agreement with the 300 hour value of K_{ISCC} determined by the modified Brown cantilever beam test ($K_{ISCC} \simeq 96$ ksi $\sqrt{in}$), as the 1000 hour value of K_{ISCC} for tube no.733 is probably lower than 96 units.

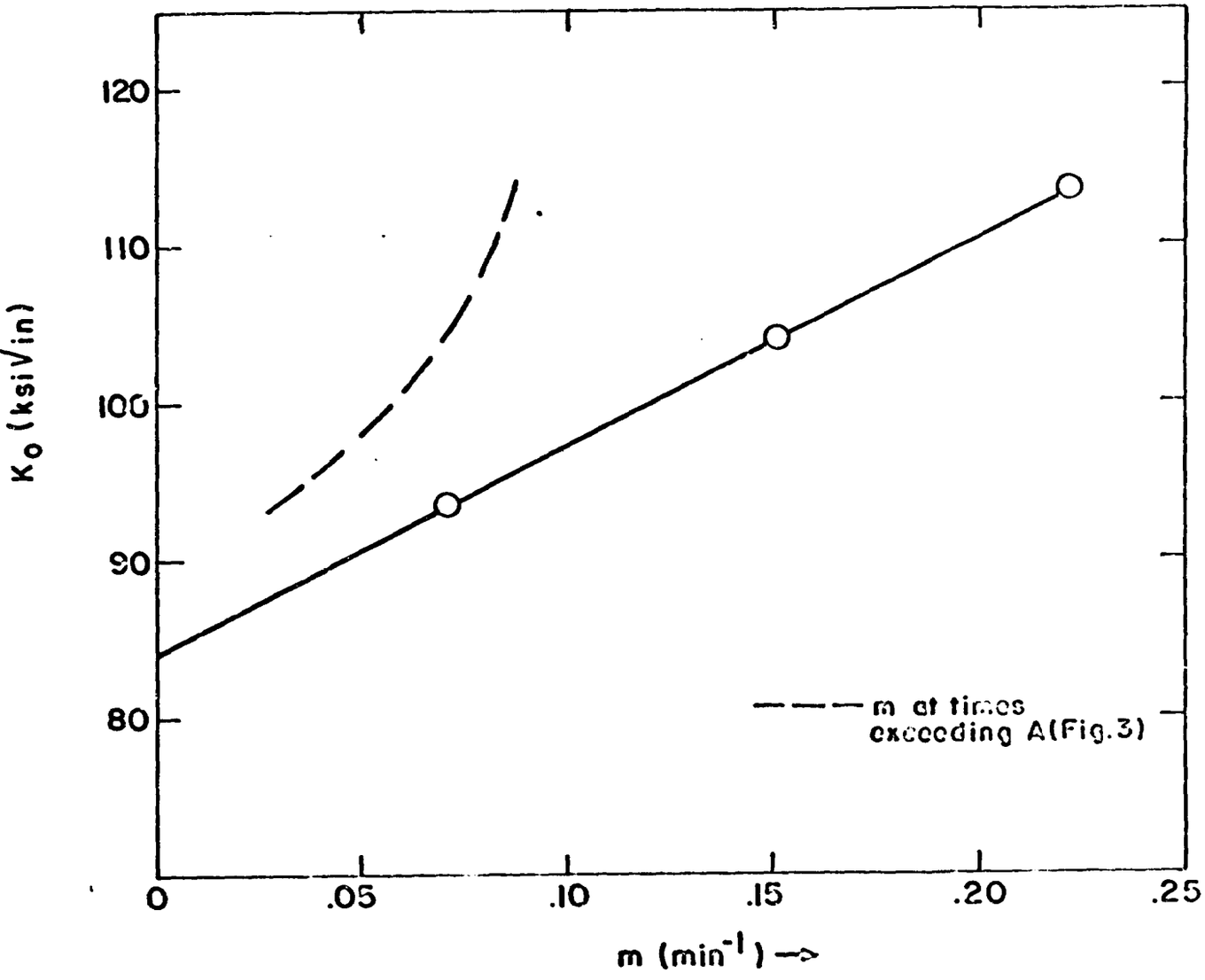

Figure 24. Variation of the Time Exponent, m, with Initial Applied Stress Intensity, K_o.

The significance of the change in slope in the plots of $\ln (\Delta a/a_o)$ vs. t for tubes no. 733 and 1007 is not yet known. The measured values of m for the second straight line portions in Figure 22 are not a linear function of K_o as shown by the dashed line in Figure 24. It is hoped that examination of electron fractographs of these specimens may indicate the cause of this behavior.

VIII. PRE-POP-IN CRACK GROWTH

A. Procedure

Precracked slow bend specimens of the program steels were instrumented for electrical potential measurements as described in Section VIID. The output of the electrical potential measuring apparatus was connected to an Esterline Angus "Speed Servo" recorder. This instrument was chosen for recording potential changes during slow bend testing because of its extremely low response time (about 0.1 second full scale). The time axis of this recorder was synchronized to the time base of the load deflection recorder by means of a marking pen activated by the on-off switch of the load deflection recorder.

Following testing, specimens were broken in impact to reveal the precrack depth. Using the method described on page 49 for converting the electrical potential data to crack length, crack growth during slow bend testing in air was obtained as a function of load and subsequently as a function of applied stress intensity.

B. Results

Figure 25 shows schematically typical load deflection and potential deflection data obtained from a slow bend test. As a typical test proceeds, an initial change in potential V is noted as the precrack separates (I to II in Figure 25). A linear change of V with deflection δ due to elastic deformation (10) (II to III) follows. Next, a second region of linear change of V with δ ensues (III to IV) and finally, V changes nonlinearly with δ (IV to fracture). The nature of the regions III to fracture was established as follows.

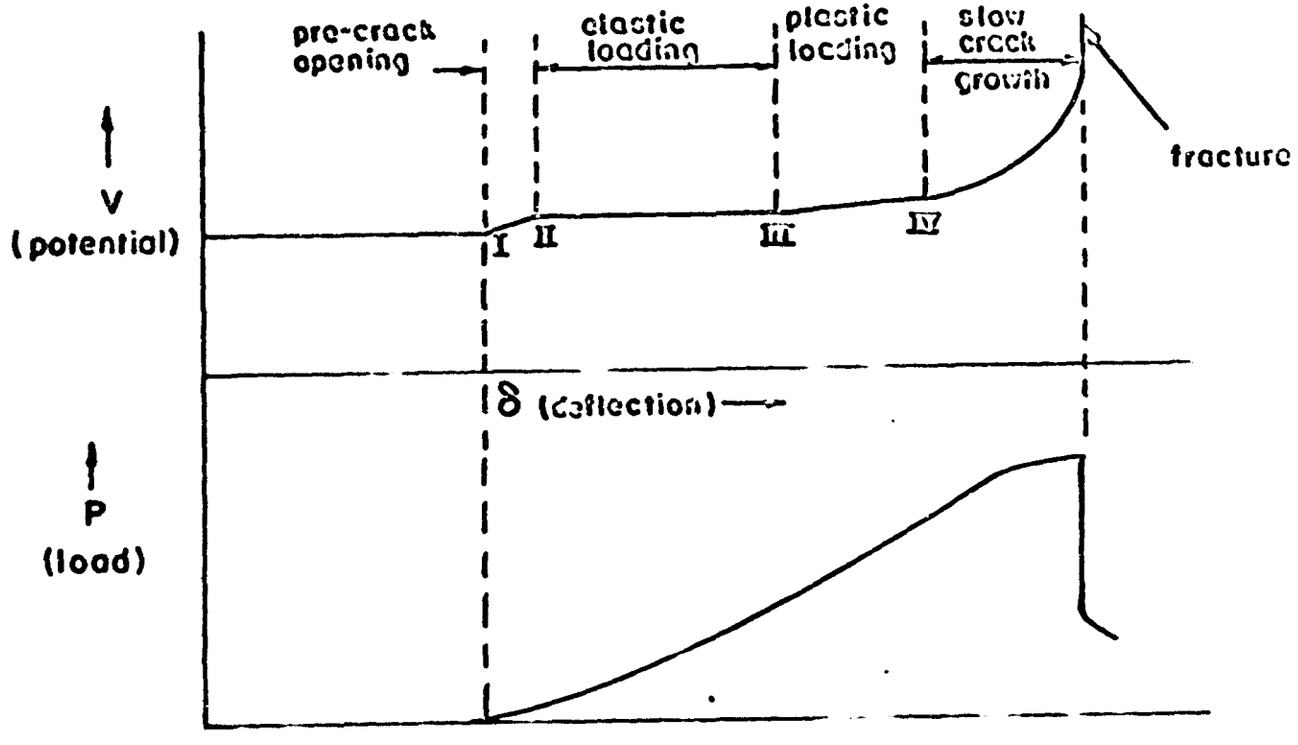

Figure 25. PRECRACK CHARPY IN SLOW BEND

Crack growth in an unprecracked bend specimen of the same dimensions was monitored by electrical potential measurement during a slow bend test (shown schematically in Figure 26). Figure 25 shows that if the load deflection record does not contain a discontinuous change in P vs. δ until crack growth has occurred, crack growth is indicated by a nonlinear change of potential with δ at IV. Furthermore, specimens loaded into the region IV to fracture and broken in impact revealed crack growth while those loaded into the region III to IV exhibited no crack growth. Thus, the identification of slow crack growth with a nonlinear change of V with δ (at the deflection rate investigated) follows directly.

The results of potential measurements during slow bend testing of PSB specimens of the program steels in air at a deflection rate of 0.0125 inch per minute are shown in Figure 26. The crosshatched area represents the stress intensity level at which slow crack growth initiated and the white area shows the level of stress intensity at which a discontinuous "pop-in" was noted on the load deformation record. The black area is the "pop-in" stress intensity level corrected by the amount of slow crack growth, as measured by electrical potential, between the onset of crack growth and "pop-in".

The stress intensity levels shown here are not intended to constitute valid K_{IC} measurements. The specimen geometry used does not satisfy the criteria for a valid K_{IC} test, but was chosen so that the results could be compared with the other impact, slow bend, corrosion fatigue, stress corrosion cracking, etc., tests involved in this program, all of which utilize the same specimen configuration. In any case, comparisons among the three gun tubes and to a more limited extent, the Marage 250 steel are meaningful.

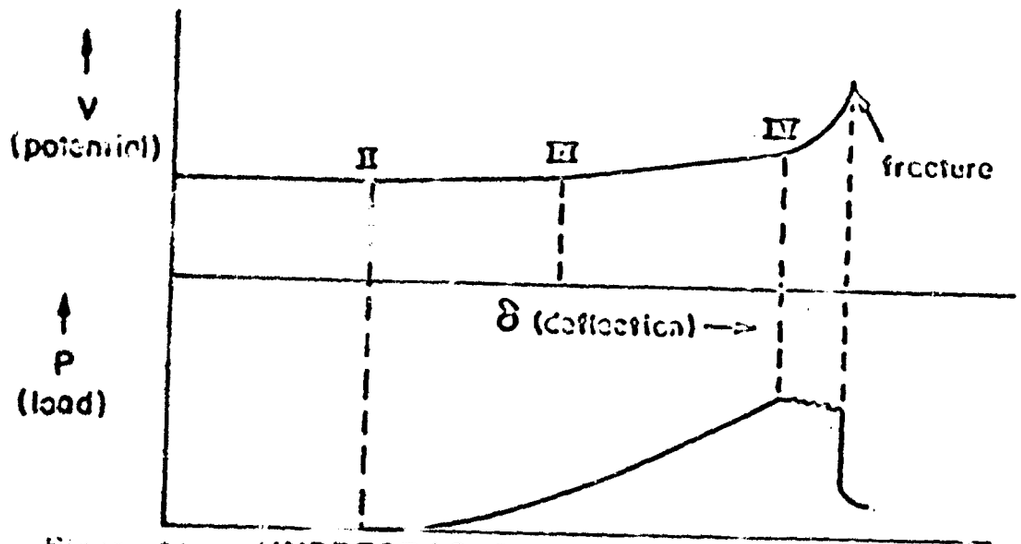

Figure 26. UNPRECRACKED CHARPY IN SLOW BEND

Figure 27 shows that the stress intensity level at macroscopic "pop-in" for the program steels correlate well with service behavior and the other fracture toughness parameters obtained in this program. However, the applied stress intensity corresponding to the onset of the pre-pop-in cracking is higher for tube no. 1007 than for tube no. 1131. Although there is as yet no explanation for this, if the difference in stress intensity between the onset of slow crack growth and macroscopic "pop-in" is taken as a measure of ability to further accommodate cracking without reaching critical stress levels, the order of increasing toughness is again Marage 250, 733, 1007, 9-4-30 and 1131.

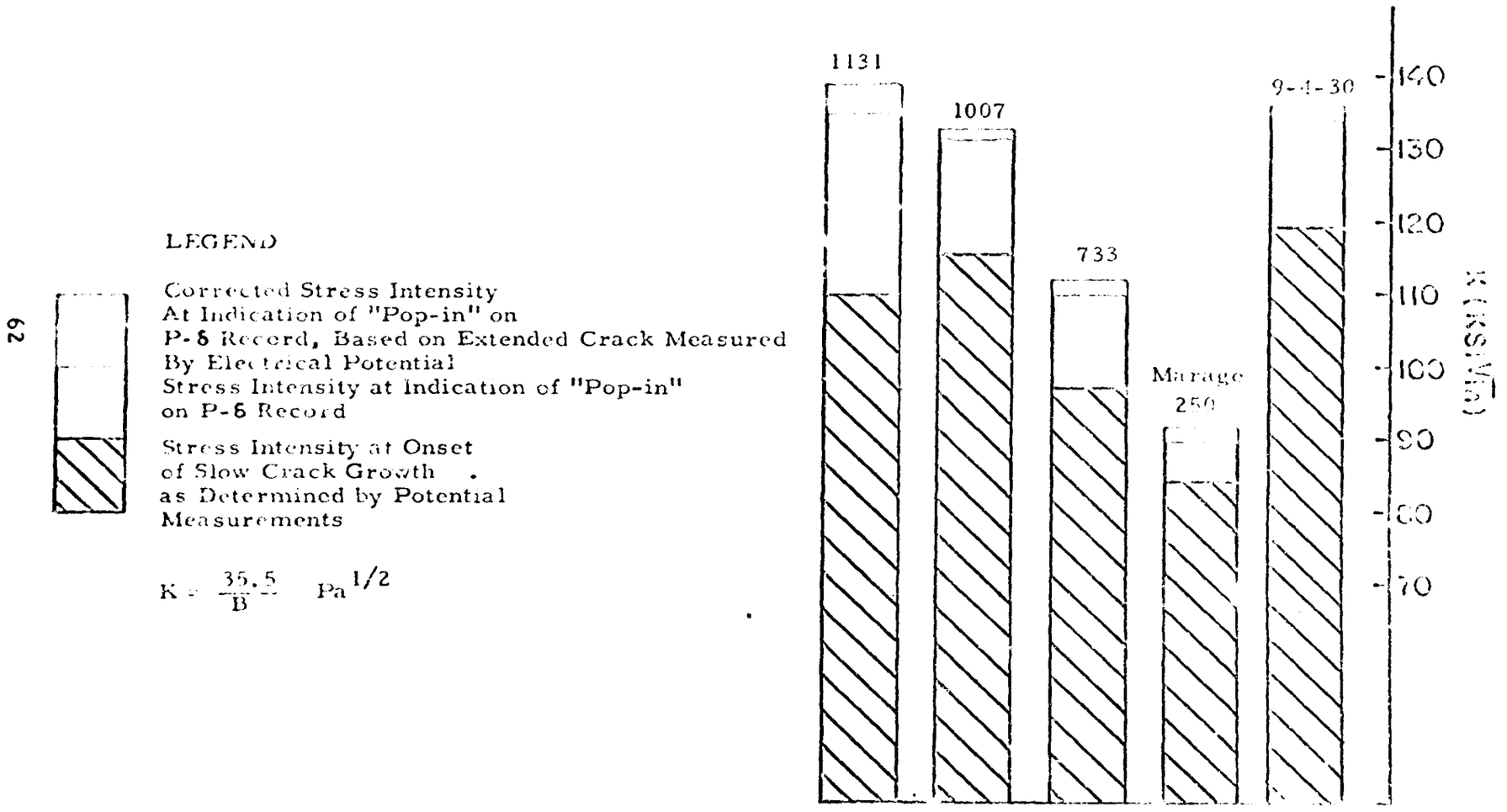

Figure 27. Pre-Pop-In Crack Growth During Slow Bend Testing of Program Steels.

IX. SUMMARY AND CONCLUSIONS

1. Gun tube no.733 was temper embrittled during production. From the information available, the embrittled condition appears to have been induced by long time tempering at 960°F. Testing also revealed that all three gun steels investigated are susceptible to temper embrittlement.

2. In low cycle, high stress fatigue of the three gun steels investigated, distilled water, as compared to dry argon, increases crack growth rates. However, in the Republic 9-4-30 and the Marage 250 steels, water has no discernible effect on crack growth rates.

3. As a result of the data obtained to date, it can be concluded that long service life is reflected by some or all of the following:

   a. high ductility
   b. high fracture toughness
   c. low ductile-brittle transition temperature
   d. high stress necessary for onset of crack growth in low cycle, high stress fatigue
   e. high values of K_{ISCC}
   f. high tolerances for crack growth after crack initiation in slow bend testing.

4. Of the three gun tubes studied, tube no.1131 consistently exhibited better performance in testing than tube no.733, with tube no.1007 being intermediate. Republic HP-9-4-30 generally exhibited properties similar to tube no.1131. Of the two steels with yield strengths different than 175-185 ksi, the Marage 250 (240 ksi yield strength) performed poorly while the Republic 9-4-20 (Cr, Mo) (160 ksi yield strength) performed exceptionally well.

5. Charpy impact testing does not reflect the ability of a steel to resist crack propagation. That portion of the energy available in a Charpy test to resist crack propagation ranged from 25 to 80% of the corresponding standard Charpy energy.

6. Crack growth in slow bend testing began before "pop-in" in all the steels investigated. The amount of additional stress intensity tolerated before "pop-in" generally correlated with higher fracture toughness levels.

X. WORK IN PROGRESS

The slow crack growth studies in this initial investigation are being continued under a short extension of the contract. At present, the following testing is underway.

1. Republic HP-9-4-20 (Cr, Mo) is being subjected to high stress low cycle fatigue testing, stress corrosion cracking testing, slow bend testing and electrical potential testing for comparison with the five steels previously investigated.

2. Testing equipment for determining the variation of potential with crack length in a corroding environment has been designed and is being constructed.

3. Low cycle high stress fatigue cycling of tubes no. 1131 and 733 at -40°F is in progress.

It is also planned to measure slow crack growth phenomena in a large number of gun tubes of known service performance in order to determine the specific parameters which correlate best with service life. It is anticipated that the latter effort will result in a standardized testing procedure for gun tube materials.

REFERENCES

1. Kalish, D. and Kulin, S. A., "Thermomechanical Treatments Applied to Ultrahigh Strength Steels", ManLabs, Inc., Final Report, Contract NOw-66-0142-c (November 1966).

2. Pellini, W. S. and Quenean, B. R., "Development of Temper Brittleness in Alloy Steels", Trans. A.S.M., 39, 193 (1947).

3. Tober, A. P., Thorlin, J. F. and Wallace, J. F., "Influence of Composition on Temper Brittleness in Alloy Steels", Trans. A.S.M., 42, 1033 (1950).

4. Low, J. R., "Temper Brittleness - A Review of Recent Work", in Trans. A.S.M., Fracture of Engineering Materials, 127 (1964).

5. McMahon, C. J., "Embrittlement of Internal Interfaces with Special Reference to Temper Embrittlement", presented at NERC Conference, "Failure of Engineering Materials", Schenectady, N. Y. (May 1967).

6. Marschall, C. W., Holden, F. C. and Hyler, W. S., "Crack Propagation at Stresses Below the Fatigue Limit", Trans. A.S.M., 60, 112 (1967).

7. Large, R. D., Lement, B. S. and Kulin, S. A., "Slow Crack Growth in Gun Tubes", ManLabs, Inc., Quarterly Report No. 1, Contract No. DA-30-144-AMC-1639(W) (November 1966).

8. Brown, B. F., "A New Stress Corrosion Cracking Test for High Strength Alloys", Materials Research Standards (March 1966) p. 129.

9. Steigerwald, E. A. and Benjamin, W. D., "Stress Corrosion Cracking Mechanism in Martensitic High Strength Steel", TRW ER 6877-3 (December 1966).

10. Anctil, A. A., Kula, E. B. and DiCesare, E., "Electrical Potential Technique for Determining Slow Crack Growth", Proc. ASTM, 63, 799 (1963).